Reviewer #1:

Overall, the authors have done a very good job of revising the manuscript and recommend that the manuscript be published with consideration of the following points about inlets:

1. Inlet characterization - Delay is only one aspect of characterization of an inlet. One can easily correct for delay simply by phase shift of the original signal. I assume that was done. I was asking that you describe the attenuation characteristics (i.e. smoothing) due to the inlet. For example, what was the e-folding time of your 'step change' in your experiment when it appeared at the detector, and how do you extrapolate that to your actual inlet?

We derived the e-folding times from a fit to step change in concentration and discussed the implications of the obtained results. For more detail on how we obtained the e-folding parameters and how we extrapolated to our actual inlet please refer as well to the new section 5 in the Supplement. We rewrote the section Discussion of inlet effects as follows:

2.4 Discussion of inlet effects

Semi-volatile and especially low-volatile compounds partition reversibly from the gas phase to the walls in Teflon tubing (Pagonis et al., 2017; Liu et al., 2019; Deming et al., 2019). Teflon tubing acts approximately as a chromatography column for these compounds (Pagonis et al., 2017). This leads to a smearing of the time profile of these compounds which affects the measured concentrations (Deming et al., 2019). To evaluate this effect we measured a step concentration change from a stable MSAM concentration to a zero MSAM concentration (at same humidity and flow). This resulting decay does not necessarily follow a single exponential decay (Liu et al., 2019). In our case we found the best fit was obtained with a triple exponential decay. The e-folding times (time it takes for the signal to decrease by the factor 1/e) were from minutes to hours (for more details see Sect. S5). This leads to considerable smoothing of the MSAM signal for concentration changes on timescales of minutes up to hours.

New added chapter in Supplement
5 Inlet characterization

We induced a concentration step change in order to determine the e-folding time (time it takes for a value to decay to 1/e) for an 1/8" teflon tubing inlet of 0.4m length. An air flow of 100sccm with a stable MSAM concentration was replaced by an air flow without MSAM (same flow and humidity). The resulting time series response (see Fig. 10) is an exponential decay which does not necessarily follow a single exponential decay [6]. A single exponential decay fit is not able to accurately fit the measured decay signal. We employed a triple exponential decay function to fit the signal S(t) (see equation 6). In this equation the parameters a, b and c added together will give the concentration at t = 0 and the parameters τ_a, τ_b and τ_c are the decay timescales. The timescale τ gives the time it takes for the signal to drop to 1/e (e-folding time). The results of the fit yield a = 18.3, b = 8.2 and c = 4.4 (unit is ppb) with τ_a = 58, τ_b = 581 and τ_c = 8561 (unit is seconds). This means that the observed exponential decay has different timescale regimes. First it decays quickly with a timescale of around one minute, then this increases to 10 minutes up to a timescale of around 142 minutes. To a good estimate the decay timescales depend proportionally on tubing length and diameter and inversely on the flow rate and saturation concentration [7]. On this basis we can estimate the decay timescales of our AQABA inlet setup (length 10m, 1/2" Teflon tubing, flow of 3slpm) to 3.3 minutes, 33 minutes and 8 hours. Therefore concentration changes happening even on timescales of half an hour or longer will be smoothed, i.e. the real variance of the concentration might have been considerably larger.

$$S(t) = a * e^{-\frac{t}{\tau_a}} + b * e^{-\frac{t}{\tau_b}} + c * e^{-\frac{t}{\tau_c}} \qquad (6)$$

There are several sentences starting at line 23 that did not make sense to me. Conclusions are made about inlet properties based on your inferences from the results - which were filtered through the inlet in the first place. That seems circular. Also, the text talks about "underestimating" the concentration - perhaps you mean "underestimating the variance in concentration"? Reporting as "lower limit" does not make sense. That is ok if ambient concentrations are increasing. If they are decreasing then smoothing in the inlet means you have reported an upper limit. Anyway, "underestimating" or "overestimating" this presumes there is no production/loss in the inlet which has not been demonstrated.

We rewrote the section concerning inlet effects to address these issues. We agree that the discussion was circular and deleted the corresponding sentences. When we stated that we underestimate the concentration we meant it as you stated it “underestimating the variance in concentration”. We agree that this was not correct to state it like that. We now state in the manuscript at the end of section 2.4:

This leads to considerable smoothing of the MSAM signal for concentration changes on timescales of minutes up to hours.

2. It is probably not reasonable to consider the inlet as a clean Teflon surface. Once sampling starts it is coated with a complex mixture of organic and inorganic aerosols, adsorbed gases, and reaction products resulting from heterogeneous chemistry. Ozone is continuously deposited to the inlet surface where it can generate ozonides, free radicals, and peroxides on the surface. H2O2 and organic peroxides are also deposited. Strong acids (nitric, sulfuric, SO2 oxidation) and ammonia (or other amines) are also present. Some teflon is also quite transparent, so photochemistry can occur (depending on the type/color of the teflon and whether it was covered.

We deleted mentioning of a clean Teflon surface. The Teflon line was covered with dark insulation material preventing photochemistry in the inlet.

Sadly, inlets are complex environments. The burden is on us atmospheric chemists to show that what we measure is not an inlet artifact. If the inlet is not characterized, then it should be acknowledged as an uncertainty for future studies to investigate. I don't think it makes sense to minimize the possibility of artifact. Numerous discoveries in atmospheric chemistry have turned out to be artifacts.

We agree that this should be stated more carefully and altered the sentences (section 2.4) accordingly to convey the message that production in the inlet (although we regard it as improbable), cannot be ruled out completely.

The partitioning of MSAM to the inside wall of the Teflon tubing raises the question whether the observed MSAM could be generated there on surfaces. No inlet test was done during the campaign to address this issue since this discovery was a surprise. We do not know of a pathway to production in the inlet (see Sect. S6 for a discussion) but it remains a possibility that cannot yet be ruled out.

3. I am not a synthetic organic chemist but I did not find the argument against formation of MSAM in the inlet to be compelling. Certainly synthesis from a sulfonic acid is unlikely, but perhaps there are

other potential precursurs. How about dimethysulfoniopropionate (DMSP)? It has a built-in S+ because it is a zwitterion. I also believe it has been reported in aerosols over the Indian Ocean. It seems more conservative to simply state that you don't know of a pathway to production on the inlet, but it remains a possibility that cannot yet be ruled out. I suppose this is a matter of style rather than fact.

In addition to the statement that production in the inlet remains a possibility (see answer to question 2 above) we moved the discussion about synthesis to the Supplement (section 6).

Reviewer #2, remaining question:

Provide a calculation of the required waterside concentration to support a gas-phase MSAM concentration of 50 ppt at typical wind speeds for the region, or state why such a calculation is not feasible.

We cannot provide an accurate calculation for the waterside concentration required as the physical conditions in the Somalia upwelling region are not known and the Henry's law constant is uncertain. However to address this comment we have included a simplified calculation of the minimum waterside concentration needed to yield a flux to the atmosphere at 50 ppt. We included this discussion in the Supplement in section 7 (see below).

7 MSAM concentration in seawater

We cannot provide an accurate calculation for the waterside concentration required as the physical conditions in the Somalia upwelling region are not known and the Henry's law constant is uncertain. Calculation of the water concentration needed to support measured atmospheric concentrations of MSAM would require a model. Due to the lack of knowledge of the conditions at the upwelling region we consider that not feasible.
However from equation 1 we can calculate the minimum MSAM water concentration (A) required to produce a positive flux to the atmosphere at a given atmospheric concentration (G). Due to the high Henry's law constant (H) compared e.g. to DMS it has to be expected that, with this two-layer model, MSAM water concentrations have to be considerably larger than DMS water concentrations in order to produce a flux to the atmosphere. Concentrations higher than $A = G * H$ *will result in a flux to the atmosphere. The water side concentration (for G =50ppt and* $H = 3.3 \times 10^4$ *M* atm^{-1}*) needs to be higher than 1700nM. This appears very high in comparison with previously reported water phase concentration of VOC [8, 4]. Measurements of water concentrations together with ambient air measurements of MSAM in an upwelling region are needed to better understand the ocean air exchange of MSAM.*

A new marine biogenic emission: methane sulfonamide (MSAM), DMS and $DMSO_2$ measured in air over the Arabian Sea

Achim Edtbauer[1], Christof Stönner[1], Eva Y. Pfannerstill[1], Matias Berasategui[1], David Walter[1,2], John N. Crowley[1], Jos Lelieveld[1,3], and Jonathan Williams[1,3]

[1]Atmospheric Chemistry Department, Max Planck Institute for Chemistry, Mainz, Germany
[2]Department Biogeochemical Processes, Max Planck Institute for Biogeochemistry, Jena, Germany
[3]Energy, Environment and Water Research Center, The Cyprus Institute, Nicosia, Cyprus

Correspondence: Achim Edtbauer (a.edtbauer@mpic.de)

Abstract. We present the first ambient measurements of a new marine emission methane sulfonamide (MSAM: CH_5NO_2S), along with dimethyl sulfide (DMS) and dimethyl sulfone ($DMSO_2$) over the Arabian Sea. Two shipborne transects (W $\rightarrow$ E, E $\rightarrow$ W) were made during the AQABA (Air Quality and Climate Change in the Arabian Basin) measurement campaign. Molar mixing ratios in picomole of species per mole of air (throughout this manuscript abbreviated as ppt) of DMS were in the range 300–500 ppt during the first traverse of the Arabian Sea (first leg) and 100–300 ppt in the second leg. In the first leg $DMSO_2$ was always below 40 ppt and MSAM was close to the limit of detection. During the second leg $DMSO_2$ was between 40–120 ppt and MSAM was mostly in the range 20–50 ppt with maximum values of 60 ppt. An analysis of HYSPLIT back trajectories combined with calculations of the exposure of these trajectories to underlying *chlorophyll* in the surface water revealed that most MSAM originates from the Somalia upwelling region, known for its high biological activity. MSAM emissions can be as high as one third of DMS emissions over the upwelling region. This new marine emission is of particular interest as it contains both sulfur and nitrogen, making it potentially relevant to marine nutrient cycling and marine atmospheric particle formation.

1 Introduction

The ocean plays an important role in the atmospheric chemistry of many trace gases and profoundly influences the global sulfur and nitrogen cycles (Brimblecombe, 2014; Sievert et al., 2007; Bentley and Chasteen, 2004; Fowler et al., 2013, 2015). Dimethyl sulphide (DMS) emitted from the ocean accounts for roughly half of the natural global atmospheric sulfate burden. The global DMS flux to the atmosphere was recently estimated to be 28.1 (17.6–34.4) Tg S per year, equivalent to 50 % of the anthropogenic sulfur inputs (Webb et al., 2019). Nitrogen is often a limiting nutrient for phytoplankton growth in the ocean (Voss et al., 2013). Nonetheless, ocean emissions of organic nitrogen do occur in the form of amines (R-NH_2) (Ge et al., 2011; Gibb et al., 1999) and in inorganic forms such as nitrous oxide (N_2O) (Arévalo-Martínez et al., 2019) and ammonia (Gibb et al., 1999; Johnson et al., 2008; Paulot et al., 2015), particularly in upwelling regions (Carpenter et al., 2012).

Upwelling regions of the ocean are those where nutrient rich waters from depths of 100 to 300 meters are brought to the surface (Voss et al., 2013; Kämpf and Chapman, 2016). Upwelling leads to nutrient richer zones in the surface ocean and therefore to regions of high phytoplankton activity, resulting in strong carbon dioxide uptake and the release of various volatile organic

compounds including sulfur, halogen and alkene containing trace gases (Arnold et al., 2010; Colomb et al., 2008; Bonsang et al., 2010; Lai et al., 2011; Yassaa et al., 2008). In the Arabian Sea, the location of this study, the Somalian coastal upwelling is a major feature. It is considered the fifth largest upwelling system in the world (deCastro et al., 2016; Ajith Joseph et al., 2019).

Here we present trace gas measurements taken on a shipborne circumnavigation of the Arabian Peninsula. Relatively few measurements have been made in this region due to political tensions and piracy. Transects of the Arabian Sea (the most southerly section of the route) showed high levels of sulfur containing gases. These include DMS, Dimethyl sulfone ($DMSO_2$) and methane sulfonamide (MSAM), a new marine emission that unusually contains both sulphur and nitrogen atoms.

DMS is known to stem from biochemical reactions within phytoplankton that produce its precursor dimethylsulphoniopropionate (DMSP) (Kiene et al., 2000). Although only a small fraction of the DMS produced within the ocean is released into the atmosphere (Vila-Costa et al., 2006), it is still the most abundant form of oceanic sulphur emission (Kloster et al., 2006; Quinn and Bates, 2011; Lana et al., 2011; Liss et al., 2014).

The oxidation mechanism of DMS in the atmosphere is complex and still not fully understood (Mardyukov and Schreiner, 2018; Barnes et al., 2006; Ayers and Gillett, 2000; Chen et al., 2018). $DMSO_2$, the second sulphur containing species measured in this study, is a product of DMS oxidation by the OH radical (Arsene et al., 2001; Barnes et al., 2006). It can be formed directly from DMS, via the intermediate dimethyl sulfoxide (DMSO) and from oxidation of DMSO with BrO and NO_3 (Barnes et al., 2006). Even though oxidation of DMS in the atmosphere is still not fully understood, reaction with the hydroxyl radical (OH) is considered the dominant loss pathway (Khan et al., 2016).

Significantly DMS oxidation ultimately yields sulfates which may act as cloud condensation nucleii (see Fig. 1). In the case of MSAM, there are no previously reported measurements of this species. The MSAM data are assessed here through comparison with the better known DMS and $DMSO_2$ species and with respect to airmass back trajectories and chlorophyll exposure, in particular in relation to the upwelling region. In summary, we examine the provenance, distribution and fate of DMS, $DMSO_2$ and the new marine emission MSAM in the region of the Arabian Sea.

2 Materials and Methods

2.1 AQABA campaign

From June 25th to September 3rd 2017, the Air Quality and Climate Change in the Arabian Basin (AQABA) cruise took place on the research vessel *Kommandor Iona*. The first leg of the cruise started from La-Seyne-sur-mer near Toulon (France), and headed through the Suez Canal, around the Arabian Peninsula and ended in Kuwait. The second leg took the same route back (see Fig. 2). Onboard the ship were a weather station and four laboratory containers equipped with instrumentation for on- and offline measurement of a large suite of trace gases, particles and radicals (Bourtsoukidis et al., 2019, 2020; Wang et al., 2020).

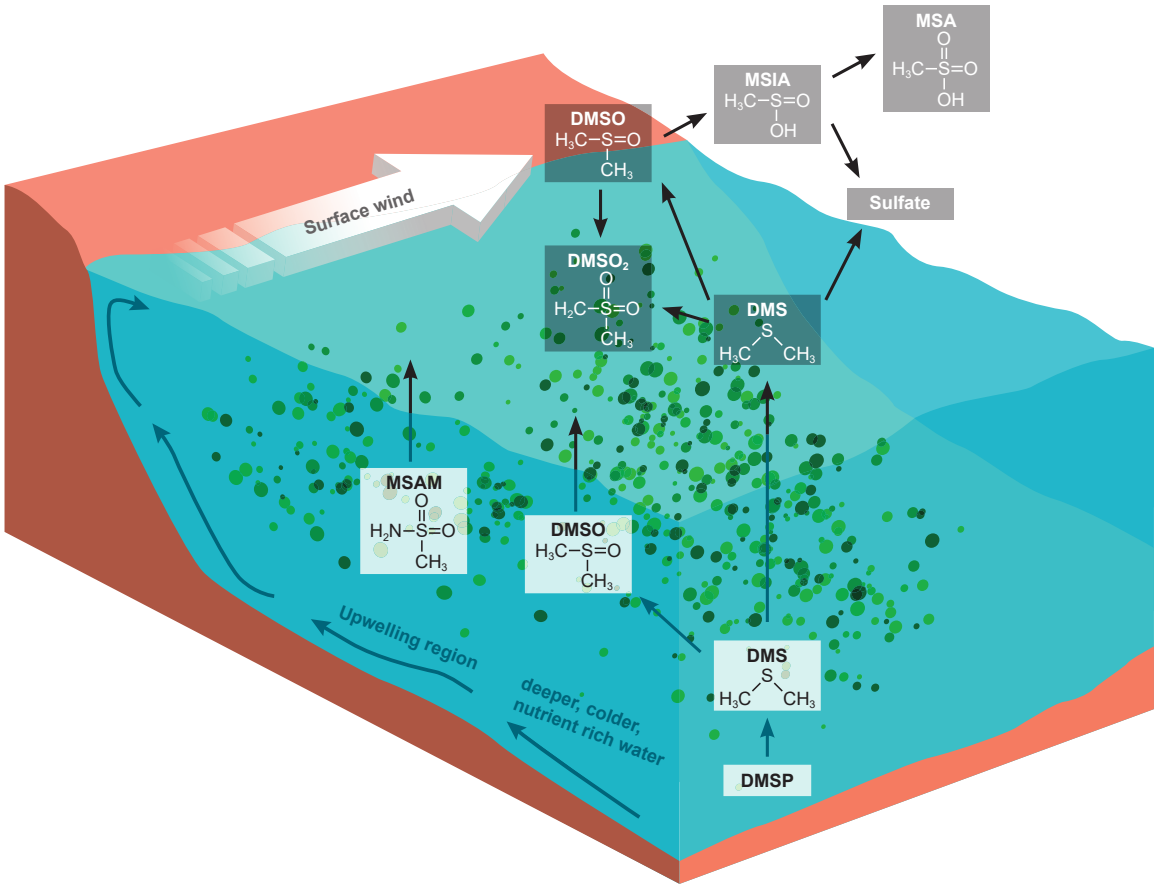

Figure 1. DMS oxidation scheme focusing on the trace gases discussed (Barnes et al., 2006). DMSP production within phytoplankton yields DMS in the surface water where it can be oxidize directly to DMSO. A small fraction of DMS is emitted to the atmosphere. Where it is predominantly oxidized by the OH radical yielding methane sulfonic acid (MSA) and sulfates. Additionally we sketched a possible formation pathways for $DMSO_2$. We suggest that MSAM could be formed in the water as a result of microbial activity and parts of it are then emitted to the atmosphere. The bottom part of the figure illustrates the principle of the Somalia upwelling. Wind blowing along the coast displaces surface water and leads to upwelling of cold nutrient rich water which can support a phytoplankton bloom (Kämpf and Chapman, 2016).

2.2 Sampling

A 10 m high (above sea level) high volume-flow inlet (HUFI) (diameter 15 cm) was used to draw ambient air down to the containers at a flow rate of 10 m^3/min. The HUFI was situated between the four containers on the foredeck so that when the ship headed into the wind no interference from the vessel's smokestack or indoor ventilation were measured. From the center of the HUFI, air was drawn continuously at a rate of ca. 5 standard liter per minute (slpm) (first leg) or 3 slpm (second leg) into an air-conditioned laboratory container via an insulated FEP (fluorinated ethylene propylene) tube (1/2" = 1.27 cm o.d., length

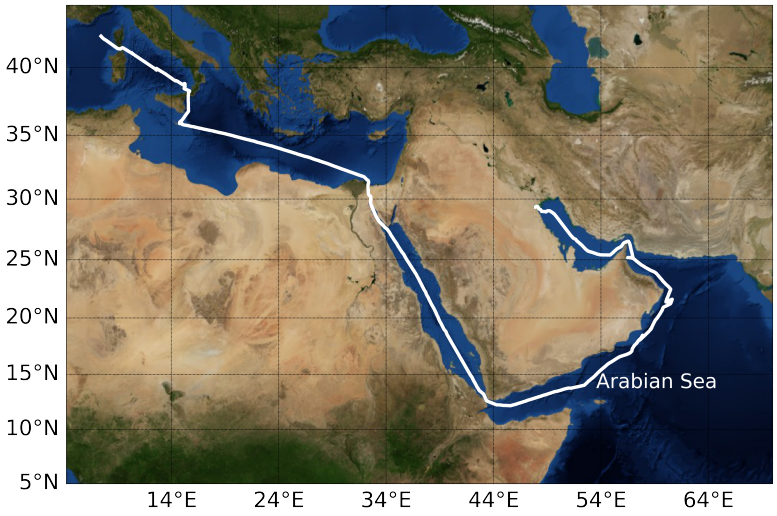

Figure 2. Ship track of AQABA cruise. Beginning of July 2017 the campaign started in the south of France near Toulon, the ship arrived in Kuwait at the end of July, started its return back to France beginning of August and was back at its starting point beginning of September 2017. On the way towards Kuwait it entered the Arabian Sea on the 19^{th} of July and left it on the 24^{th} of July. On the way back it entered the Arabian Sea on the 11^{th} of August and left it on the 15^{th} of August. Credit: NASA Earth Observatory.

ca. 10 m). The tube was heated to 50–60 °C to avoid condensation inside the air-conditioned container. To prevent sampling of sea spray and particles, a routinely changed PTFE (polytetrafluorethylene) filter was installed in the inlet line before it entered the container. This inlet system was employed for the measurements of VOCs and total OH reactivity (Pfannerstill et al., 2019) simultaneously. The inlet residence time for the VOC measurements was determined by a spiking test with acetone, and was 12 s during the first leg and 26 s during the second leg.

2.3 Volatile Organic Compounds (VOCs) measurements

Online volatile organic compounds (VOCs) measurements were performed using a proton transfer reaction time-of-flight mass spectrometer (PTR-TOF-MS 8000, Manufacturer: Ionicon Analytik GmbH, Innsbruck, Austria). Detailed descriptions of the instrument can be found in Jordan et al. (2009); Graus et al. (2010); Veres et al. (2013). Drift pressure was maintained at 2.2 mbar and the drift voltage at 600 V (E/N 137 Td). For mass scale calibrations, 1,3,5-trichlorobenzene was continuously fed into the sample stream. The PTR-TOF-MS was calibrated at the beginning, during and at the end of the campaign (in total five humidity dependent calibrations were conducted as described by Derstroff et al. (2017)). Calibrations were performed by using a standard gas mixture (Apel-Riemer Environmental inc., Broomfield, USA) of several VOCs with gravimetrically determined

mixing ratios. The VOCs included in the calibration gas were: methanol, acetonitrile, acetaldehyde, acetone, dimethyl sulfide, isoprene, methyl vinyl ketone, methacrolein, methyl ethyl ketone, benzene, toluene, o-xylene, 1,3,5-trimethylbenzene and α-pinene. Clean synthetic air was measured every three hours for ten minutes to determine the instrument background. Synthetic air was supplied to the instrument only and not the whole inlet. The time resolution of the measurement was 1 minute and the mass range extended to 450 amu. Mass resolution (full width half maximum) at mass 96 amu was ca. 3500 during the first leg and > 4500 during the second leg.

The total uncertainty of the DMS measurement was < 30% (main sources of uncertainty: standard gas mixture 5 %, flow meter 1 %, calibration ≈ 10 %), and the precision < 5 %. $DMSO_2$ and MSAM were not present in the calibration gas. Calculation of the mixing ratio was therefore conducted based on the rate coefficients for proton transfer (Su and Chesnavich, 1982; Chesnavich et al., 1980), the knowledge of transmission factors, amount of H_3O^+ ions and parameters of the drift region (Lindinger et al., 1998). Applying this method results in a greater uncertainty than for compounds included in the calibration gas mixture of approximately 50 %. The limit of detection (LOD: 3×standard deviation of background) was 20 ppt for DMS, 25 ppt for $DMSO_2$ and 5 ppt for MSAM.

2.4 Discussion of inlet effects

Semi-volatile and especially low-volatile compounds ~~can partition~~ partition reversibly from the gas phase to the walls in Teflon tubing ~~and therefore delay the instrument response to~~ (Pagonis et al., 2017; Liu et al., 2019; Deming et al., 2019). Teflon tubing acts approximately as a chromatography column for these compounds (Pagonis et al., 2017). ~~The delay in instrument response caused by the inlet can be measured by applying a step concentration change and determination~~ This leads to a smearing of the time ~~it takes for the compound signal response to reach 90 % of the final signal response. We therefore performed tests with step concentration changes of MSAM in the laboratory. After~~ profile of these compounds which affects the measured concentrations (Deming et al., 2019). To evaluate this effect we measured a step concentration change ~~the delay time was about 2 minutes for a~~ from a stable MSAM concentration to a zero MSAM concentration (at same humidity and flow). This resulting decay does not necessarily follow a single exponential decay (Liu et al., 2019). In our case we found the best fit was obtained with a triple exponential decay. The e-folding times (time it takes for the signal to decrease by the factor 1/~~8" Teflon inlet of 0.4 m in length and a flow rate of 100 sccm. It is known that the delay depends proportionally on tubing length and diameter and inversely on the flow rate and saturation concentration (Pagonis et al., 2017). On this basis we can estimate the delay time of our AQABA inlet setup (length 10 m, 1/2" Teflon tubing, flow~~e) were from minutes to hours (for more details see Sect. S5). This leads to considerable smoothing of the MSAM signal for concentration changes on timescales of ~~3 slpm)to ≈ 7 minutes. This implies that larger concentration changes on timescales of minutes will be underestimated for $DMSO_2$ and MSAM. In this paper we show that $DMSO_2$ and MSAM originated from the Somalia upwelling and not from local sources around the ship. Therefore, we do not expect abrupt concentration changes on the timescale of minutes. Even if the delay of $DMSO_2$ and MSAM through the inlet was considerably longer than estimated it would be still sufficient to measure accurately the concentration since these species were detected over considerably longer time periods. We will only underestimate if large changes of concentration happen on timescales close to the inlet delay time. To take account of such~~

~~circumstances, that we cannot rule out completely, we state that the reported molar mixing ratios are considered to be a lower limit~~minutes up to hours.

The partitioning of MSAM to the inside wall of the Teflon tubing raises the question whether the observed MSAM could be generated there on surfaces. No inlet test was done during the campaign to address this issue since this discovery was a surprise. ~~Therefore, we cannot rule out completely that such an effect occurs. However we do consider it highly unlikely that MSAM was formed via a surface reaction of $DMSO_2$ (or an analogous species) with NH_3 or NH_4^+ . $DMSO_2$ as well as NH_3 and NH_4^+ are both very unreactive molecules and the interaction would be taking place on a non-catalytic Teflon surface. Additionally, we see no way of how NH_4^+ and NH_3 could lose their hydrogen atoms in order to form the requisite NH_2 group. A chemical synthesis pathway for sulfonamides from sulfonic acids has been published (de Luca and Giacomelli, 2008). The first step towards the production of MSAM would be removal of the whole OH group of methane sulfonic acid (MSA), creating a $CH_3SO_2^+$ ion. In an aqueous solution, the preferred reaction is, however, the removal of H^+, i.e. forming $CH_3SO_3^-$~~We do not know of a pathway to production in the inlet (see Sect. S6 for a discussion) but it remains a possibility that cannot yet be ruled out. ~~In this chemical synthesis, aggressive reagents such as trichlorotriazine and high energy (e.g. from a microwave) are used to create an intermediate CH_3SO_2Cl which reacts as a $CH_3SO_2^+$ ion. In the second step, this $CH_3SO_2^+$ ion reacts with an amine (for MSAM formation this would need to be replaced by NH_3) in a strong basic solution (NaOH(aq)), abstracting an H from NH_3 to form MSAM. The fact that sulfonic acids and not sulfones are used as precursors in synthesis of sulfonamides points outthat formation from sulfones is either not possible or more difficult than with sulfonic acids. Formation of MSAM therefore needs aggressive reagents, input of energy and strong basic conditions which were not present in our inlet.~~

2.5 HYSPLIT back trajectories

Air mass back trajectories were calculated to investigate the origin of air masses encountered. The Hybrid Single-Particle Lagrangian Integrated Trajectory model (HYSPLIT, version 4, 2014), a hybrid between a Lagrangian and an Eulerian model for tracing small imaginary air parcels forward or back in time (Draxler and Hess, 1998), was used to derive 3D back trajectories from a starting height of 200 m above sea level, going 216 hours back in time on an hourly grid beginning at the ship position.

3 Results

This study focuses on the two crossings of the Arabian Sea during the AQABA campaign. The Arabian Sea was generally characterized by low values of VOCs, especially VOCs related to anthropogenic activities (Bourtsoukidis et al., 2019, 2020; Pfannerstill et al., 2019; Wang et al., 2020). The three molecules presented in this study are the exception. They were higher in the Arabian Sea region than in the other regions. So the absence or very low concentrations of the other molecules plus the high values (compared to other regions) of DMS, $DMSO_2$ and MSAM characterize this part of the cruise as mostly influenced by clean marine air.

3.1 Dimethyl sulfide (DMS)

Measurements of DMS (m/z 63.0263) during AQABA showed elevated mixing ratios when the vessel traversed the Arabian Sea during both legs (brown shaded region in Fig. 3 a). During the first leg over the Arabian Sea (Fig. 3 b), DMS mixing ratios were generally in the range of 300–500 ppt, with occasional peaks of 800 ppt. During the second leg (Fig. 3 c), the DMS mixing ratios over the Arabian Sea were significantly lower in the range of 100–300 ppt, again with elevated peaks of short duration (around 2 h).

3.2 Dimethyl sulfone ($DMSO_2$)

$DMSO_2$ was measured by the PTR-ToF-MS at m/z 95.0161. Within the range of uncertainty for that mass we did not find another plausible molecular structure. Additionally, the head space of the pure compound (TCI Deutschland GmbH, purity > 99 %) was sampled yielding a peak at the same position as found in ambient air. Measurements of $DMSO_2$ in the Arabian Sea region showed elevated levels between 40–120 ppt during the second leg (Fig. 3 c)) but more modest levels (< 40 ppt) in leg 1 (Fig. 3 b)). To our knowledge, there have been no measurements of $DMSO_2$ performed in this region previously.

3.3 New atmospheric trace gas: Methane sulfonamide (MSAM)

At m/z 96.0144, a signal was observed which displayed a strong correlation with $DMSO_2$ (Pearson correlation coefficient: r around 0.8) over the Arabian sea during the second leg (see Fig. 4). This mass corresponded to methane sulfonamide (MSAM), which has a similar structure to $DMSO_2$, with an amine group substituted for a methyl group (see Fig. 1 for the chemical structures of the molecules). This molecule has not previously been measured in ambient air. To confirm the assignment of mass m/z 96.0144 to MSAM, the head-space of the pure substance MSAM (Alfa Aesar, purity > 98 %) was sampled by the PTR-ToF-MS. The analysis of the pure compound MSAM by PTR-ToF-MS matched the mass found in ambient air. No other plausible molecular structures could be found for this mass within the uncertainty for that mass. Based on the correlation of mass m/z 96.0144 to $DMSO_2$ in ambient data, the mass spectral match to the pure compound, and the absence of alternative structures at that exact mass we identify the measured signal as MSAM. In order to test whether MSAM can be observed outgassing from seawater, we flushed the headspace of solutions of 4.2 mol L^{-1}, 0.05 mol L^{-1} and 0.0005 mol L^{-1} MSAM in artificial seawater with 100, 50 and 25 ml min^{-1} of synthetic air (Air Liquide, Krefeld, Germany) each. The resulting mixing ratios measured ranged from 650 ppt (lowest concentration and lowest flow rate) to 130000 ppt (highest concentration and highest flow rate). Up to a certain flow value the increase in dilution due to an increase in flow is overcompensated through an enhanced emission of the substance from the seawater. Therefore we measured the highest MSAM mixing ratios at the highest flow rate. During the Arabian Sea section of the second leg, values of up to 60 ppt were measured, but mostly it was found in the range of 20–50 ppt. In the first leg, MSAM was occasionally detected in the Arabian Sea, but concentrations were generally close to the LOD.

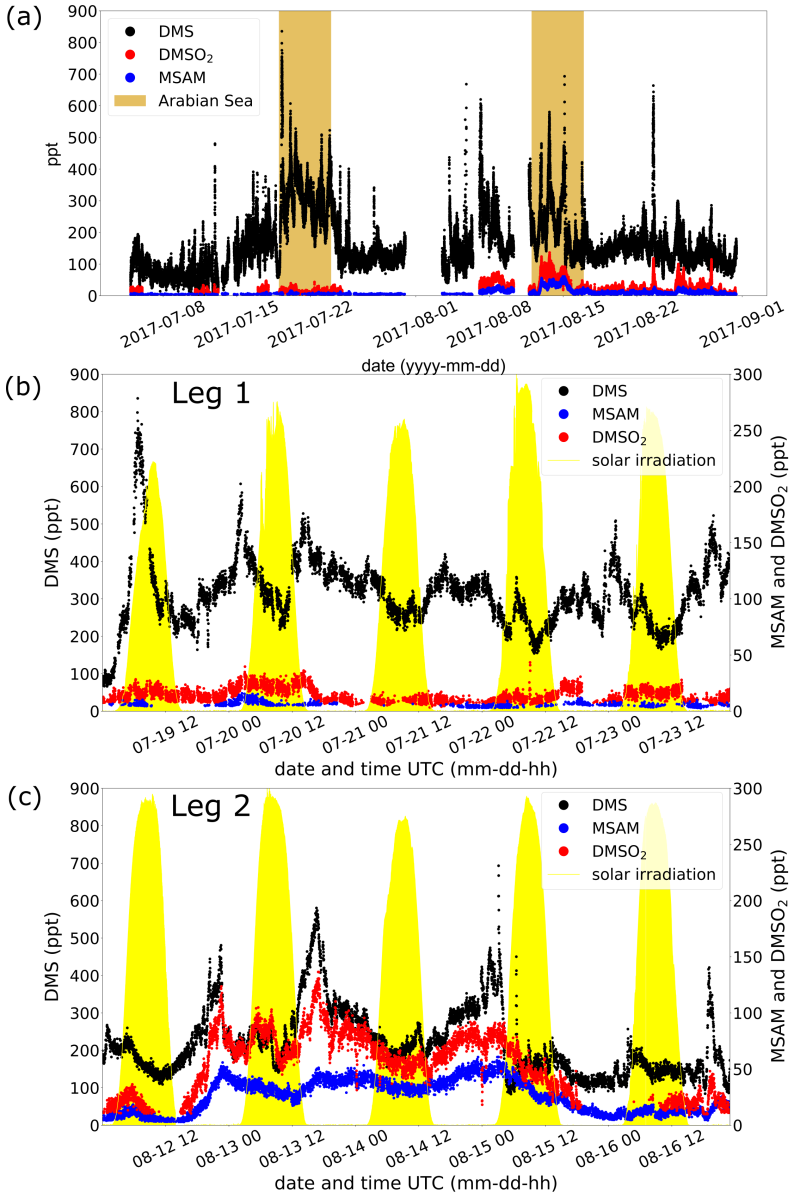

Figure 3. In panel (a) the mixing ratios of for DMS, $DMSO_2$ and MSAM during the whole AQABA cruise are displayed. The Arabian Sea parts of leg 1 and 2 are marked with brown. A zoom-in on measurements over the Arabian Sea is given for leg 1 in panel (b) and for leg 2 in panel (c). The yellow filled curves in panels (b,c) show the solar irradiation in arbitrary units.

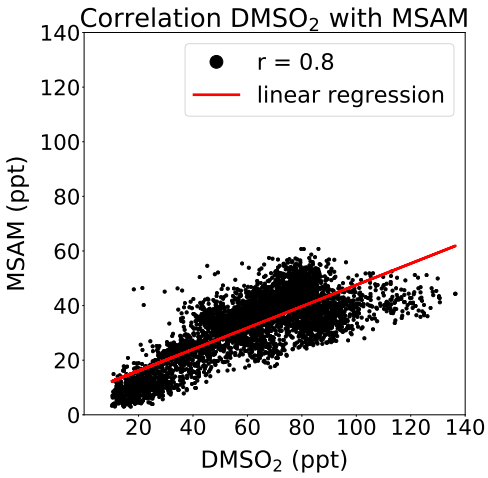

Figure 4. Correlation of MSAM with $DMSO_2$ during the second leg in the Arabian Sea. Displayed in red the is the linear regression ($[\text{MSAM}] = 0.393 * [\text{DMSO}_2] + 8.245$ ppt). The Pearson correlation coefficient is 0.8.

4 Discussion

Here we discuss DMS, $DMSO_2$ and MSAM measurements in air from a rarely sampled region, the Arabian Sea. First we discuss the difference in DMS abundance between the two legs. Secondly we evaluate the source regions of these trace gases based on knowledge of their atmospheric lifetimes and chlorophyll exposure. Then finally we address the implications of these measurements to marine boundary layer chemistry.

4.1 DMS

We observed higher values of DMS in July (leg 1) than in August (leg 2) over the Arabian Sea (see 3.1). This finding is consistent with DMS fluxes predictions by Lana et al. (2011) for this region. Sea surface DMS concentrations can be used to estimate DMS fluxes to the atmosphere and a global climatology of DMS surface water concentrations has been derived by Lana et al. (2011) from over 47000 seawater measurements worldwide. Lana et al. (2011) predict strong fluxes of DMS in the Arabian Sea region, particularly in June, July and August, coincident with the AQABA campaign. Seawater concentration data for DMS from the Lana climatology relevant for AQABA has been plotted in Fig. 5 for July and August. In the regions south of the Arabian Peninsula, higher concentrations of DMS in seawater are expected in July than in August. Therefore the measured higher mixing ratios of DMS in July than August are supporting the results of the climatology for this region.

The highest DMS mixing ratios occurred during the first leg over the Gulf of Aden with around 800 ppt. The peak values are likely related to the ship crossing directly through patches of phytoplankton as evidenced by the observation of strong bioluminescence around the ship during the night. The DMS mixing ratio values of up to 300 ppt during the second leg can be

compared to measurements made previously in that region. DMS values up to 250 ppt associated with upwelling in the Gulf of Aden were reported during a ship cruise in April 2000 (Warneke and de Gouw, 2001). More recent measurements during a ship cruise in July and August 2018 in the western tropical Indian Ocean reported values of up to 300 ppt DMS (Zavarsky et al., 2018). The DMS measurements presented here are therefore consistent with the very limited previous measurements in this region.

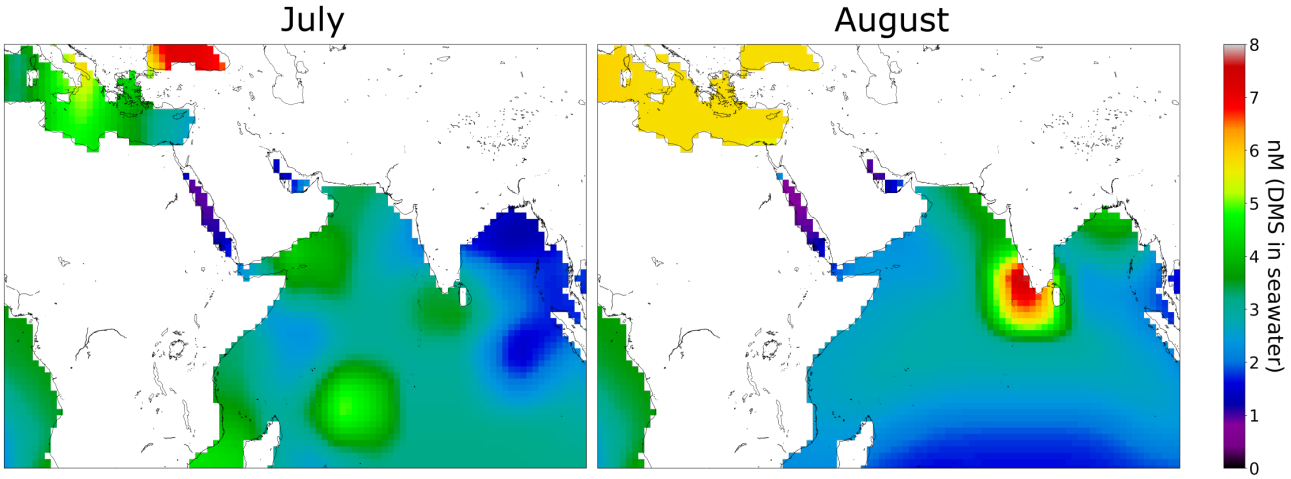

Figure 5. Climatology for DMS surface water concentrations in July and August (Lana et al., 2011). Over 47 000 DMS seawater measurements were used together with interpolation/extrapolation techniques in order to obtain a monthly DMS surface water concentration of the whole earth. In the regions south of the Arabian Peninsula the climatology estimates higher values in July than in August.

4.2 Atmospheric lifetimes of DMS, $DMSO_2$ and MSAM

The lifetime of DMS in the atmosphere with respect to the primary oxidant OH is around 1.3 days (bimolecular rate constant = 7.8×10^{-12} cm^3 molec^{-1} s^{-1} (Albu et al., 2006)). For all lifetimes with respect to OH we use the global average concentration [OH] = 1.1×10^6 molec/cm^3 (Prinn et al., 2005). In some regions of the marine boundary layer, BrO may also contribute to the oxidation of DMS leading to shorter DMS lifetimes (Breider et al., 2010; Khan et al., 2016; Barnes et al., 2006).

The reaction rate of OH and $DMSO_2$ is $< 3 \times 10^{-13}$ cm^3 molec^{-1} s^{-1}, which leads to a tropospheric lifetime of more than 35 days ([OH] = 1.1×10^6 molec/cm^3) (Falbe-Hansen et al., 2000), over twenty times longer than DMS. A recent study Berasategui et al. (2020) measured a rate constant of $1.4 \pm (0.2) \times 10^{-13}$ cm^3 molec^{-1} s^{-1} for the reaction of OH with MSAM, which results in a tropospheric lifetime of 75 days ([OH] = 1.1×10^6 molec/cm^3). As MSAM has a long lifetime with respect to reaction with OH, we must also consider its physical removal by deposition to the ocean surface. We therefore carried out experiments to determine the Henry's law constant for MSAM (details see Sect. S2) and found it to be in the range 3.3×10^4 M atm^{-1}–6.5×10^5 M atm^{-1}. $DMSO_2$ has a similarly large Henry's law constant $> 5 \times 10^4$ M atm^{-1} (de Bruyn et al., 1994). A two-layer model can predict the exchange flux between the gas and aqueous phase to derive an estimate of the effective lifetimes

(Liss and Slater, 1974; Schwartz, 1992; Yang et al., 2014). For substances with a high Henry's law constant, like MSAM and $DMSO_2$, knowledge of the wind speed and the marine boundary layer height is sufficient to get a prediction of the deposition lifetime (details see Sect. S1). This gives a lifetime of 30.5 ± 23.5 hours (marine boundary layer height: 750 ± 250 meters and wind speeds 4 m s^{-1} to 14 m s^{-1}). The lifetimes for MSAM and $DMSO_2$ are therefore controlled by the deposition rate to the ocean surface and not by OH oxidation. This means that DMS, $DMSO_2$ and MSAM have similar lifetimes. During August the 12^{th} and 13^{th}, airmasses from the Somalia upwelling most of the time traveled for 10 h up to a day before reaching the ship. On the 14^{th} and 15^{th} of August, airmasses from the Somalia upwelling were around 4 h old (determined from the HYSPLIT back trajectories). A common oceanic source and the similar lifetimes of $DMSO_2$ and MSAM help explain the observed good correlation of MSAM with $DMSO_2$ (see Fig. 4).

4.3 Chlorophyll exposure of HYSPLIT back trajectories

MSAM and $DMSO_2$ were close to the LOD during the first leg, despite the fact that DMS mixing ratios were even higher than during the second leg. This observation excludes a simple relationship between the emissions of DMS and $DMSO_2$/MSAM. $DMSO_2$ is known to be an oxidation product of DMS and is therefore linked to marine biogenic activity (Barnes et al., 2006). We hypothesize that the newly detected trace gas MSAM is also linked to marine biogenic activity. This is based on the observation that MSAM displays the highest values when influenced mainly by remote marine air without recent contact with land, it correlates well with $DMSO_2$ (see Fig. 4 (c)) and is similar in chemical structure to DMS and $DMSO_2$. A good indicator for marine biogenic activity is phytoplankton. Phytoplankton in the water can be detected from space via the *chlorophyll a* pigment used for photosynthesis. Satellite images of regional chlorophyll can be exploited to investigate emission areas of marine biogenic VOCs. In the following sections we will investigate, with the help of HYSPLIT back trajectories and *chlorophyll a* water content, where the source of MSAM and $DMSO_2$ is located.

4.3.1 *Chlorophyll a* water content

We used data from the satellite MODIS-aqua (Jackson et al., 2019). In Fig. 6 a,b and d,e) the *chlorophyll a* concentration averaged over 8 days is plotted for the time periods relevant for our measurements. During the first leg (Fig. 6 a, b) the ship entered the Arabian Sea region on the 19^{th} of July and left it around the 23^{rd} of July 2017. Figure 6 a) displays the average chlorophyll distribution from the 12^{th} until the 19^{th} of July, since air masses reaching the ship from July 19^{th} onwards will have traveled over *chlorophyll a* regions before the time of observation. For the second leg (Fig. 6 d,e) (12^{th} of August till the 16^{th} of August 2017) we used the average *chlorophyll a* content from the 5^{th} of August till the 12^{th} of August and from the 13^{th} till the 20^{th} of August. The highest chlorophyll concentrations in the region are found off the Horn of Africa/Somalia coast, a strong upwelling region.

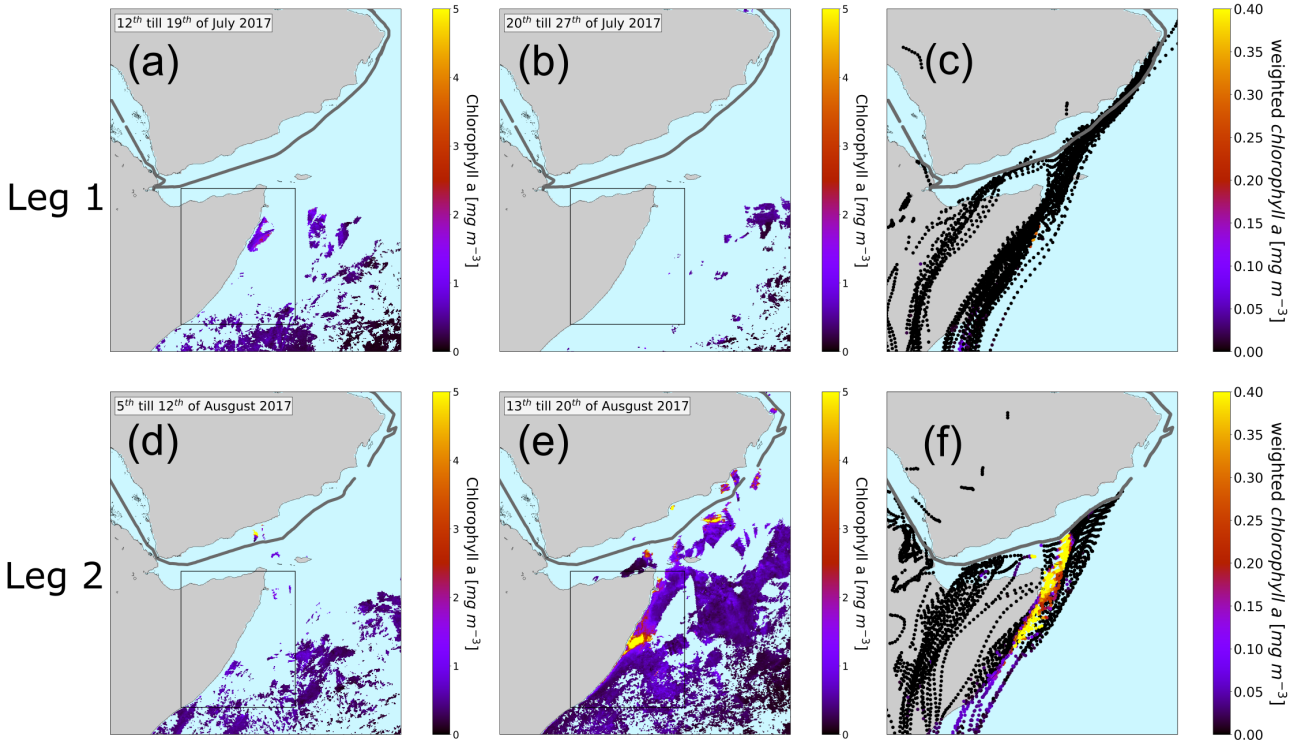

Figure 6. Eight day averaged *chlorophyll a* concentration in the Arabian Sea. The relevant time periods for the first leg (a,b) and for the second leg (d,e) are pictured here. Plot (a) represents the average *chlorophyll a* concentration from the 12^{th} until the 19^{th} of July, plot (b) from the 20^{th} until the 27^{th} of July, plot (d) from the 5^{th} till the 12^{th} of August and plot (e) from the 13^{th} till the 20^{th} of August. The black rectangle represents the region of the Somalia coast upwelling. The ship track is plotted in gray. The light blue means no *chlorophyll a* content. Plots (c) and (f) display the HYSPLIT back trajectories. The color code of the trajectories represents the weighted amount of *chlorophyll a* concentration in the water underneath the trajectory.

4.3.2 Back-trajectory-chlorophyll analysis

A trajectory analysis was carried out to investigate whether air masses traveling over regions of high chlorophyll are associated with higher atmospheric levels of $DMSO_2$, and MSAM. To investigate the provenance of air-masses sampled at the ship in relation to the chlorophyll distributions shown above, HYSPLIT back-trajectories were calculated (9 days back) for every full hour of the cruise. For each point of the trajectory the underlying *chlorophyll a* content was weighted with respect to the arrival time at the ship to account for oxidation and dispersion effects (see Fig. 6 c and f). These values were then added up for each trajectory individually in order to determine quantitatively to what extent the air sampled had passed over areas of high chlorophyll content (indicator for phytoplankton in the water). Only time points when the trajectory was within the marine boundary layer, as calculated from the HYSPLIT model, were considered. Changing of the weighting did not materially affect

the results. For details on the weighting procedure see Sect. S3.

The results of these calculations are displayed in Fig. 7. The graphs show the total chlorophyll exposure and the exposure

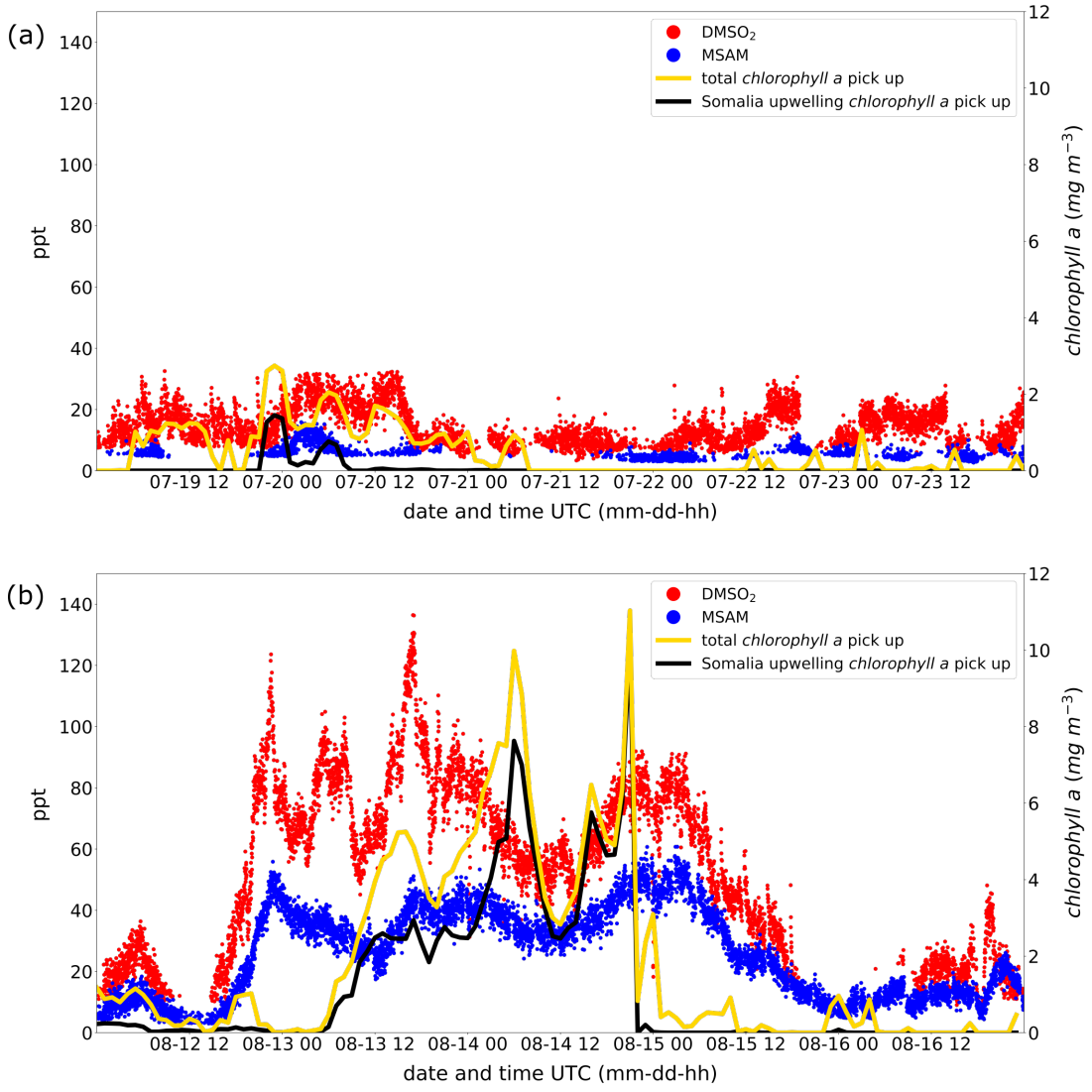

Figure 7. Weighted amount of *chlorophyll a* trajectories crossed over before arrival at the ship for leg 1 (a) and leg 2 (b). The total *chlorophyll a* exposure (yellow line) and the *chlorophyll a* exposure originating from the Somalia upwelling region (black line) is plotted. The corresponding y-axis for the *chlorophyll a* exposure for both graphs (a,b) is displayed on the right side. Mixing ratios in ppt for $DMSO_2$ and MSAM are plotted in red and blue with the corresponding y-axis on the left side.

of chlorophyll specifically from the region of the Somalia upwelling (see Fig. 6 the region in the black rectangle). In the first leg (Fig. 7 (a)), when both $DMSO_2$ and MSAM mixing ratios were low, air reaching the ship did not cross *chlorophyll a* rich

waters in the previous 1 to 2 days. This is the case for the total exposure as well as for the exposure to chlorophyll in the Somalia upwelling region.

However, during the second leg (Fig. 7 (b)), when $DMSO_2$ and MSAM levels were high, the air measured had traveled over extensive *chlorophyll a* rich waters. In general, the exposure in the Somalia upwelling region always constituted the majority of the total exposure, except for one peak in the beginning (August 13^{th} from 12:00 till 19:00) where chlorophyll patches closer to the ship constituted roughly half of the total chlorophyll exposure. From these calculations we can conclude that the occurrence of $DMSO_2$ and MSAM is related to marine emissions in the Somalia upwelling region. MSAM and $DMSO_2$ mixing ratios started to increase around midday of August 12^{th} but the chlorophyll exposure only started to increase around 6:00 on August 13^{th} (Fig. 7 (b)). A possible explanation for the delay in chlorophyll exposure could be that the bloom already started on August 12^{th} and not just on August 13^{th} as indicated in Fig. 6 d,e. Possibly the earlier start of the bloom escaped detection by MODIS-aqua as it sees every point on earth every 1–2 days. Around the equator some regions escape detection on any given day. An inspection of daily data from MODIS-aqua revealed that parts of the Somalia upwelling were in a blind spot of the satellite on August 12^{th}. The chlorophyll exposure sharply fell to zero at the beginning of the 15^{th} of August, roughly 8 h before $DMSO_2$ and MSAM values start to decline as well (Fig. 7 (b)). In this case the calculated HYSPLIT back-trajectories no longer pass over the Somalia upwelling but cross Somalia before arriving at the ship. Our measurements thus indicate that we were impacted by the Somalian upwelling region for longer than calculated from the trajectories. This is not unexpected as meteorological data for this region are sparse, and the trajectories therefore correspondingly uncertain.

4.4 $DMSO_2$, DMSO, MSIA and MSA

In the following we will discuss briefly why we did not detect DMSO, MSIA and methane sulfonic acid (MSA). These are important oxidation products from DMS.

DMSO is known to be an important intermediate in the oxidation of DMS with OH (Hoffmann et al., 2016). The reaction rate of DMSO with OH is 15 times faster than that of DMS with OH, making it a potentially important sink in the remote marine atmosphere (Barnes et al., 2006). A model study of the sulfur cycle in the global marine atmosphere suggested values of around 10 ppt for DMSO in the region of the Arabian Sea (Chen et al., 2018). This is below the limit of detection (LOD) of around 15 ppt for DMSO in our instrument and probably the reason why we do not observe it in this dataset. Measurements of DMSO made on Amsterdam Island ranged from 0.36 to 11.6 ppt (Sciare et al., 2000).

MSIA has a very high reaction rate of 9×10^{-11} cm^3 $molec^{-1}$ s^{-1} with OH radicals (Burkholder et al., 2015; Kukui et al., 2003; Hoffmann et al., 2016). In the model study mentioned above, this leads to concentrations over the Arabian Sea of around 2 ppt which again is below the LOD for MSIA with our instrument (around 20 ppt) (Chen et al., 2018).

MSA, on the other hand, is predicted to be around 20–40 ppt over the Arabian Sea (gas phase and aqueous phase combined), which is above its LOD, but almost all of it will be in the aqueous phase (Chen et al., 2018; Hoffmann et al., 2016). In the gas phase, the maximum MSA values reported to date are below 1 ppt, which is far too low to be measured with our setup (LOD around 15 ppt) (Eisele and Tanner, 1993; Chen et al., 2016; Berresheim, 2002).

We observed $DMSO_2$ mixing ratios during the second leg between 40 and 120 ppt, which is high compared to previous measurements of 0.2–11 ppt (Berresheim et al., 1998; D. Davis et al., 1998) made in Antarctica. In the following we will shortly describe and discuss formation pathways for $DMSO_2$. This will be done for formation via OH, BrO and NO_3.

4.4.1 OH

$DMSO_2$ formation from OH oxidation, via the intermediate DMSO, has been observed in laboratory studies (Falbe-Hansen et al., 2000). However it has to be noted that newer studies indicate that mainly methane sulfinic acid (MSIA) and not $DMSO_2$ is formed (Barnes et al., 2006; Kukui et al., 2003; Hoffmann et al., 2016). Another pathway is formation from the OH-DMS adduct followed by sequential reactions with NO and O_2 (Arsene et al., 2001; Barnes et al., 2006). Due to the low NO_x of the remote marine atmosphere this pathway seems unlikely as well. There are speculations about a possible formation from the initial formed OH-DMS adduct by O_2 addition and a subsequent complex process which is not yet fully understood (Berndt and Richters, 2012; Arsene et al., 1999; Turnipseed et al., 1996; Barnes et al., 2006).

4.4.2 BrO

BrO can form $DMSO_2$ from DMSO. But these reaction seems rather unlikely because of the slow reaction rate compared to the fast reaction rate of OH and DMSO. This reaction therefore would only play a role for much higher concentrations of BrO and not for concentrations of 2 ppt for BrO, which have been proposed to be ubiquitous in the marine troposphere (Read et al., 2008; Platt and Hönninger, 2003).

4.4.3 NO_3

Most studies show no formation of $DMSO_2$ from NO_3 oxidation (Barnes et al., 2006). NO_3 oxidation of the intermediate DMSO is known to only yield $DMSO_2$ (Falbe-Hansen et al., 2000). However, NO_3 oxidation is not thought to produce DMSO (Barnes et al., 2006). Maybe the increase in $DMSO_2$ after sunset (see Fig. 3 c) is an indication that NO_3 is oxidizing the remaining DMSO from OH oxidation of DMS produced during daytime.

With the data presented here it is not possible to decide if one or some of the above mentioned mechanisms are responsible for the observed $DMSO_2$ values. A diel analysis of DMS, MSAM and $DMSO_2$ was made. But due to the fact that we only have two consecutive days with elevated $DMSO_2$ on a moving platform the results must be viewed with caution since variation may come from source or removal process variation. Nevertheless, for completeness the plots and description of these diel variability plots are in the supplement (see Sect. S4).

4.5 MSAM

We are not aware of a possible formation pathway for MSAM in the gas phase. Therefore we consider it rather unlikely that it is formed via DMS gas phase oxidation. A microbial formation from DMS or DMS products in the water of the highly biological

active upwelling region with subsequent emission into the atmosphere seems plausible (see Fig. 1).

To our knowledge there have been no reports of MSAM occurring or being produced in biological systems. MSAM belongs to the class of sulfonamides which is known for its antibacterial properties and it has therefore been used in antibacterial drugs (Sköld, 2010). The only mentioning of MSAM in this context was as a metabolite of a drug detected in human urine (Anacardio et al., 2009).

From the dataset presented in this paper, the ocean is expected to be a sink for MSAM. This is shown through our calculations of the lifetime (few hours to a few days) which are dominated by deposition. The ocean can only become a source of MSAM to the atmosphere if the concentration of MSAM in surface seawater is so large that emission locally dominates over deposition. Our measurements indicate that this was the case in the region of the Somalia upwelling. Although, no seawater measurements were made in that region to confirm this, the trajectory data presented here indicate that biologically active areas are able to produce sufficiently large MSAM concentrations.

To our knowledge, no measurements of MSAM have been reported in the atmosphere so far and thus no information about the potential role it could play there is available. SO_2 is an oxidation product of MSAM (Berasategui et al., 2020) and a precursor for sulfuric acid (H_2SO_4). H_2SO_4 is known to be a key contributor to new particle formation (Li et al., 2018; Kulmala et al., 2014; Almeida et al., 2013; Sipilä et al., 2010; Weber et al., 2001, 1996; Chen et al., 2016). However, due to the slow reaction of MSAM with OH, the contribution of MSAM to SO_2 is negligible (Berasategui et al., 2020). Acid-base reactions (e.g. H_2SO_4 with ammonia/amines) are very important in new particle formation (Chen and Finlayson-Pitts, 2017; Almeida et al., 2013). MSAM is an acid and therefore could participate in acid-base reactions, but since MSAM is only a weak acid ($pK_a = 10.8$ (Junttila and Hormi, 2009)) its role as an acid in these reactions is probably limited.

Studies indicate, that the dominant driving force in new particle formation and growth are the hydrogen bonds formed between common atmospheric nucleation precursors (Xie et al., 2017; Cheng et al., 2017; Li et al., 2018). The newly found trace gas MSAM is very intriguing because it contains a sulfonamide group, which is a sulfonyl group connected to an amine group. The sulfonyl and the amine group both support hydrogen bonding, giving MSAM a high hydrogen-bonding capacity, potentially enabling nucleation.

Because of the comparable lifetimes of MSAM and DMS, we can estimate the relative emission of MSAM to DMS from the ratio of the mixing ratios of ([MSAM]/[DMS]). We only included ratios observed in the afternoons of 14^{th} and 15^{th} of August, when the ship was in closest proximity to the Somalia upwelling. The afternoon was chosen to make sure that both MSAM and DMS have roughly the same atmospheric lifetime when estimating the relative emission. Deposition to the ocean surface will happen all the time for MSAM however OH, the main loss process for DMS, is only present during the day. We derived ratios ranging from 0.1 to 0.27, meaning that emissions of MSAM over the Somalia upwelling can be almost a third of the DMS emissions. Therefore, MSAM could play an important role in particle formation and/or growth over and downwind of upwelling regions. To verify these possibilities, further experiments regarding particle growth and formation with MSAM need to be performed.

5 Conclusions

During the AQABA campaign we made the first measurements of MSAM in ambient air. Back-trajectories-chlorophyll analyses suggest that it is a marine biogenic emission from the highly productive upwelling region off Somalia. During the first leg of the AQABA campaign the ship encountered mostly biogenic emissions from sources located along the ship route when crossing the Arabian Sea. The enhanced DMS values observed there could be attributed to seasonally enhanced DMS fluxes. No oxidation products or other organosulfur compounds were detected in substantial amounts from the local emissions. In contrast, during the second leg not only DMS but also $DMSO_2$ and MSAM were measured. $DMSO_2$, like MSAM, was shown to originate from the Somalia upwelling region. $DMSO_2$ mixing ratios of up to 120 ppt were measured during the second leg, which is quite substantial considering that previous studies indicate it to be a minor or negligible product in DMS gas phase oxidation. The main loss mechanism for MSAM and $DMSO_2$ is deposition to the ocean surface with lifetimes of a few hours to a few days. MSAM is a molecule which, to our knowledge, was never reported in the atmosphere. We detected it in concentrations up to 60 ppt during the second leg in the Arabian Sea. Emissions of MSAM over the Somalia upwelling can reach close to a third of the DMS emissions.

A marine emission containing a nitrogen atom is somewhat surprising since under most circumstances primary productivity in the ocean is nitrogen limited. The emission of a nitrogen containing compound may be related to the abundance of reactive nitrogen provided by the upwelling. Due to its sulfonyl and amine group, MSAM has a high hydrogen-bonding capacity enabling hydrogen bonding to other atmospheric nucleation precursors. These hydrogen bonds are known to be a critical factor in particle growth and formation (Li et al., 2018; Xie et al., 2017; Cheng et al., 2017). Therefore MSAM could prove to be of importance for particle formation and/or growth over upwelling regions. The mechanisms in which gas phase precursors lead to new particle formation is an active research area in atmospheric chemistry because it is subject to large uncertainties (Li et al., 2018; Chen et al., 2016, 2018; Carslaw et al., 2013).

Data availability. Data available via: https://dx.doi.org/10.17617/3.3o

Author contributions. AE and CS were responsible for VOC measurements and data. AE analysed the data and drafted the article. EP contributed laboratory experiments concerning Henry's law constant. MB and JC contributed to data interpretation. DW calculated the back trajectories. JL designed and realized the campaign. JW supervised the study. All authors contributed to manuscript writing and revision, read and approved the submitted version.

Competing interests. The authors declare that they have no conflict of interest.

Disclaimer. TEXT

Acknowledgements. We thankfully acknowledge the cooperation with the Cyprus Institute (CyI), the King Abdullah University of Science and Technology (KAUST) and the Kuwait Institute for Scientific Research (KISR). We thank Hays Ships Ltd, Captain Pavel Kirzner and the ship crew for their support on-board the Kommandor Iona. We would like to express our gratitude to the whole AQABA team, particularly Hartwig Harder for daily management of the campaign; and Marcel Dorf, Claus Koeppel, Thomas Klüpfel and Rolf Hofmann for logistical organization and help with preparation and setup. We are thankful to Jan Schuladen for the J-value measurements, Ulrike Weis for providing artificial seawater and Tom Jobson and Franziska Köllner for helpful discussions. The campaign was funded by the Max Planck Society.

References

Ajith Joseph, K., Jayaram, C., Nair, A., George, M. S., Balchand, A. N., and Pettersson, L. H.: Remote Sensing of Upwelling in the Arabian Sea and Adjacent Near-Coastal Regions, in: Remote sensing of the Asian Seas, edited by Barale, V. and Gade, M., vol. 92, pp. 467–483, Springer, Cham, Switzerland, https://doi.org/10.1007/978-3-319-94067-0_26, 2019.

Albu, M., Barnes, I., Becker, K. H., Patroescu-Klotz, I., Mocanu, R., and Benter, T.: Rate coefficients for the gas-phase reaction of OH radicals with dimethyl sulfide: temperature and O2 partial pressure dependence, Physical Chemistry Chemical Physics, 8, 728–736, https://doi.org/10.1039/B512536G, https://pubs.rsc.org/en/content/articlepdf/2006/cp/b512536g, 2006.

Almeida, J., Schobesberger, S., Kürten, A., Ortega, I. K., Kupiainen-Määttä, O., Praplan, A. P., Adamov, A., Amorim, A., Bianchi, F., Breitenlechner, M., David, A., Dommen, J., Donahue, N. M., Downard, A., Dunne, E., Duplissy, J., Ehrhart, S., Flagan, R. C., Franchin, A., Guida, R., Hakala, J., Hansel, A., Heinritzi, M., Henschel, H., Jokinen, T., Junninen, H., Kajos, M., Kangasluoma, J., Keskinen, H., Kupc, A., Kurtén, T., Kvashin, A. N., Laaksonen, A., Lehtipalo, K., Leiminger, M., Leppä, J., Loukonen, V., Makhmutov, V., Mathot, S., McGrath, M. J., Nieminen, T., Olenius, T., Onnela, A., Petäjä, T., Riccobono, F., Riipinen, I., Rissanen, M., Rondo, L., Ruuskanen, T., Santos, F. D., Sarnela, N., Schallhart, S., Schnitzhofer, R., Seinfeld, J. H., Simon, M., Sipilä, M., Stozhkov, Y., Stratmann, F., Tomé, A., Tröstl, J., Tsagkogeorgas, G., Vaattovaara, P., Viisanen, Y., Virtanen, A., Vrtala, A., Wagner, P. E., Weingartner, E., Wex, H., Williamson, C., Wimmer, D., Ye, P., Yli-Juuti, T., Carslaw, K. S., Kulmala, M., Curtius, J., Baltensperger, U., Worsnop, D. R., Vehkamäki, H., and Kirkby, J.: Molecular understanding of sulphuric acid–amine particle nucleation in the atmosphere, Nature, 502, 359–363, https://doi.org/10.1038/nature12663, https://www.nature.com/articles/nature12663.pdf, 2013.

Anacardio, R., Mullins, F. G. P., Hannam, S., Sheikh, M. S., O'Shea, K., Aramini, A., D'Anniballe, G., D'Anteo, L., Ferrari, M. P., and Allegretti, M.: Development and validation of an LC-MS/MS method for determination of methanesulfonamide in human urine, Journal of chromatography. B, Analytical technologies in the biomedical and life sciences, 877, 2087–2092, https://doi.org/10.1016/j.jchromb.2009.05.051, 2009.

Arévalo-Martínez, D. L., Steinhoff, T., Brandt, P., Körtzinger, A., Lamont, T., Rehder, G., and Bange, H. W.: N2O Emissions From the Northern Benguela Upwelling System, Geophysical Research Letters, 46, 3317–3326, https://doi.org/10.1029/2018GL081648, https://agupubs.onlinelibrary.wiley.com/doi/full/10.1029/2018GL081648, 2019.

Arnold, S. R., v. Spracklen, D., Gebhardt, S., Custer, T., Williams, J., Peeken, I., and Alvain, S.: Relationships between atmospheric organic compounds and air-mass exposure to marine biology, Environmental Chemistry, 7, 232, https://doi.org/10.1071/EN09144, 2010.

Arsene, C., Barnes, I., and Becker, K. H.: FT-IR product study of the photo-oxidation of dimethyl sulfide: Temperature and O2 partial pressure dependence, Physical Chemistry Chemical Physics, 1, 5463–5470, https://doi.org/10.1039/a907211j, 1999.

Arsene, C., Barnes, I., Becker, K. H., and Mocanu, R.: FT-IR product study on the photo-oxidation of dimethyl sulphide in the presence of NOx—temperature dependence, Atmospheric Environment, 35, 3769–3780, https://doi.org/10.1016/S1352-2310(01)00168-6, 2001.

Ayers, G. P. and Gillett, R. W.: DMS and its oxidation products in the remote marine atmosphere: implications for climate and atmospheric chemistry, Journal of Sea Research, pp. 275–286, 2000.

Barnes, I., Hjorth, J., and Mihalopoulos, N.: Dimethyl sulfide and dimethyl sulfoxide and their oxidation in the atmosphere, Chemical reviews, 106, 940–975, https://doi.org/10.1021/cr020529, 2006.

Bentley, R. and Chasteen, T. G.: Environmental VOSCs–formation and degradation of dimethyl sulfide, methanethiol and related materials, Chemosphere, 55, 291–317, https://doi.org/10.1016/j.chemosphere.2003.12.017, 2004.

Berasategui, M., Amedro, D., Edtbauer, A., Williams, J., Lelieveld, J., and Crowley, J. N.: Kinetic and mechanistic study of the reaction between methane sulfonamide (CH₃S(O)₂NH₂) and OH, Atmospheric Chemistry and Physics, 20, 2695–2707, https://doi.org/10.5194/acp-20-2695-2020, 2020.

Berndt, T. and Richters, S.: Products of the reaction of OH radicals with dimethyl sulphide in the absence of NOx: Experiment and simulation, Atmospheric Environment, 47, 316–322, https://doi.org/10.1016/j.atmosenv.2011.10.060, http://www.sciencedirect.com/science/article/pii/S1352231011011538, 2012.

Berresheim, H.: Gas-aerosol relationships of H 2 SO 4 , MSA, and OH: Observations in the coastal marine boundary layer at Mace Head, Ireland, Journal of Geophysical Research, 107, 24,191, https://doi.org/10.1029/2000JD000229, 2002.

Berresheim, H., Huey, J. W., Thorn, R. P., Eisele, F. L., Tanner. D. J., and Jefferson, A.: Measurements of dimethyl sulfide, dimethyl sulfoxide, dimethyl sulfone, and aerosol ions at Palmer Station, Antarctica, Journal of Geophysical Research, 1998, 1629–1637, 1998.

Bonsang, B., Gros, V., Peeken, I., Yassaa, N., Bluhm, K., Zoellner, E., Sarda-Esteve, R., and Williams, J.: Isoprene emission from phytoplankton monocultures: the relationship with chlorophyll-a, cell volume and carbon content, Environmental Chemistry, 7, 554, https://doi.org/10.1071/EN09156, 2010.

Bourtsoukidis, E., Ernle, L., Crowley, J. N., Lelieveld, J., Paris, J.-D., Pozzer, A., Walter, D., and Williams, J.: Non-methane hydrocarbon (C₂–C₈) sources and sinks around the Arabian Peninsula, Atmospheric Chemistry and Physics, 19, 7209–7232, https://doi.org/10.5194/acp-19-7209-2019, https://www.atmos-chem-phys.net/19/7209/2019/acp-19-7209-2019.pdf, 2019.

Bourtsoukidis, E., Pozzer, A., Sattler, T., Matthaios, V. N., Ernle, L., Edtbauer, A., Fischer, H., Könemann, T., Osipov, S., Paris, J.-D., Pfannerstill, E. Y., Stönner, C., Tadic, I., Walter, D., Wang, N., Lelieveld, J., and Williams, J.: The Red Sea Deep Water is a potent source of atmospheric ethane and propane, Nature Communications, 11, 447, https://doi.org/10.1038/s41467-020-14375-0, 2020.

Breider, T. J., Chipperfield, M. P., d. Richards, N. A., Carslaw, K. S., Mann, G. W., and v. Spracklen, D.: Impact of BrO on dimethylsulfide in the remote marine boundary layer, Geophysical Research Letters, 37, https://doi.org/10.1029/2009GL040868, https://agupubs.onlinelibrary.wiley.com/doi/full/10.1029/2009GL040868, 2010.

Brimblecombe, P.: The Global Sulfur Cycle, in: Treatise on geochemistry, edited by Holland, H. D., pp. 559–591, Elsevier, Amsterdam, https://doi.org/10.1016/B978-0-08-095975-7.00814-7, 2014.

Burkholder, J. B., Sander, S. P., Abbatt, J., Barker, J. R., Huie, R. E., Kolb, C. E., Kurylo, M. J., Orkin, V. L., Wilmouth, D. M., and Wine, P. H.: Chemical Kinetics and Photochemical Data for Use in Atmospheric Studies, Evaluation Number 18, JPL Publication 15-10, Jet Propulsion Laboratory, Pasadena, https://doi.org/10.13140/RG.2.1.2504.2806, 2015.

Carpenter, L. J., Archer, S. D., and Beale, R.: Ocean-atmosphere trace gas exchange, Chemical Society reviews, 41, 6473–6506, https://doi.org/10.1039/c2cs35121h, 2012.

Carslaw, K. S., Lee, L. A., Reddington, C. L., Pringle, K. J., Rap, A., Forster, P. M., Mann, G. W., v. Spracklen, D., Woodhouse, M. T., Regayre, L. A., and Pierce, J. R.: Large contribution of natural aerosols to uncertainty in indirect forcing, Nature, 503, 67, https://doi.org/10.1038/nature12674, https://www.nature.com/articles/nature12674.pdf, 2013.

Chen, H. and Finlayson-Pitts, B. J.: New Particle Formation from Methanesulfonic Acid and Amines/Ammonia as a Function of Temperature, Environmental science & technology, 51, 243–252, https://doi.org/10.1021/acs.est.6b04173, 2017.

Chen, H., Varner, M. E., Gerber, R. B., and Finlayson-Pitts, B. J.: Reactions of Methanesulfonic Acid with Amines and Ammonia as a Source of New Particles in Air, The journal of physical chemistry. B, 120, 1526–1536, https://doi.org/10.1021/acs.jpcb.5b07433, 2016.

Chen, Q., Sherwen, T., Evans, M., and Alexander, B.: DMS oxidation and sulfur aerosol formation in the marine troposphere: a focus on reactive halogen and multiphase chemistry, Atmospheric Chemistry and Physics, 18, 13 617–13 637, https://doi.org/10.5194/acp-18-13617-2018, 2018.

Cheng, S., Tang, S., Tsona, N. T., and Du, L.: The Influence of the Position of the Double Bond and Ring Size on the Stability of Hydrogen Bonded Complexes, Scientific reports, 7, 11 310, https://doi.org/10.1038/s41598-017-11921-7, https://www.nature.com/articles/s41598-017-11921-7.pdf, 2017.

Chesnavich, W. J., Su, T., and Bowers, M. T.: Collisions in a noncentral field: A variational and trajectory investigation of ion–dipole capture, The Journal of Chemical Physics, 72, 2641–2655, https://doi.org/10.1063/1.439409, 1980.

Colomb, A., Yassaa, N., Williams, J., Peeken, I., and Lochte, K.: Screening volatile organic compounds (VOCs) emissions from five marine phytoplankton species by head space gas chromatography/mass spectrometry (HS-GC/MS), Journal of environmental monitoring : JEM, 10, 325–330, https://doi.org/10.1039/b715312k, 2008.

D. Davis, G. Chen, P. Kasibhatla, A. Jefferson, D. Tanner, F. Eisele, D. Lenschow, W. Neff, and H. Berresheim: DMS oxidation in the Antarctic marine boundary layer: Comparison of model simulations and held observations of DMS, DMSO, DMSO<subscr>2</subscr>, H<subscr>2</subscr>SO<subscr>4</subscr>(g), MSA(g), and MSA(p), Journal of Geophysical Research, 1998, 1657–1678, 1998.

de Bruyn, W. J., Shorter, J. A., Davidovits, P., Worsnop, D. R., Zahniser, M. S., and Kolb, C. E.: Uptake of gas phase sulfur species methanesulfonic acid, dimethylsulfoxide, and dimethyl sulfone by aqueous surfaces, Journal of Geophysical Research: Atmospheres, 99, 16 927–16 932, https://doi.org/10.1029/94JD00684, https://agupubs.onlinelibrary.wiley.com/doi/full/10.1029/94JD00684, 1994.

de Luca, L. and Giacomelli, G.: An easy microwave-assisted synthesis of sulfonamides directly from sulfonic acids, The Journal of organic chemistry, 73, 3967–3969, https://doi.org/10.1021/jo800424g, 2008.

deCastro, M., Sousa, M. C., Santos, F., Dias, J. M., and Gómez-Gesteira, M.: How will Somali coastal upwelling evolve under future warming scenarios?, Scientific reports, 6, 30 137, https://doi.org/10.1038/srep30137, 2016.

Deming, B. L., Pagonis, D., Liu, X., Day, D. A., Talukdar, R., Krechmer, J. E., de Gouw, J. A., Jimenez, J. L., and Ziemann, P. J.: Measurements of delays of gas-phase compounds in a wide variety of tubing materials due to gas–wall interactions, Atmospheric Measurement Techniques, 12, 3453–3461, https://doi.org/10.5194/amt-12-3453-2019, 2019.

Derstroff, B., Hüser, I., Bourtsoukidis, E., Crowley, J. N., Fischer, H., Gromov, S., Harder, H., Janssen, R. H. H., Kesselmeier, J., Lelieveld, J., Mallik, C., Martinez, M., Novelli, A., Parchatka, U., Phillips, G. J., Sander, R., Sauvage, C., Schuladen, J., Stönner, C., Tomsche, L., and Williams, J.: Volatile organic compounds (VOCs) in photochemically aged air from the eastern and western Mediterranean, Atmospheric Chemistry and Physics, 17, 9547–9566, https://doi.org/10.5194/acp-17-9547-2017, 2017.

Draxler, R. R. and Hess, G.: An Overview of the HYSPLIT _ 4 Modelling System for Trajectories , Dispersion , and Deposition, Australian Meteorological Magazine, pp. 295–308, https://pdfs.semanticscholar.org/b534/55cef2115b8b26cb1deb44d3dccb1b5e0d16.pdf, 1998.

Eisele, F. L. and Tanner, D. J.: Measurement of the gas phase concentration of H 2 SO 4 and methane sulfonic acid and estimates of H 2 SO 4 production and loss in the atmosphere, Journal of Geophysical Research, 98, 9001–9010, https://doi.org/10.1029/93JD00031, 1993.

Falbe-Hansen, H., Sørensen, S., Jensen, N. R., Pedersen, T., and Hjorth, J.: Atmospheric gas-phase reactions of dimethylsulphoxide and dimethylsulphone with OH and NO3 radicals, Cl atoms and ozone, Atmospheric Environment, 34, 1543–1551, https://doi.org/10.1016/S1352-2310(99)00407-0, 2000.

Fowler, D., Coyle, M., Skiba, U., Sutton, M. A., Cape, J. N., Reis, S., Sheppard, L. J., Jenkins, A., Grizzetti, B., Galloway, J. N., Vitousek, P., Leach, A., Bouwman, A. F., Butterbach-Bahl, K., Dentener, F., Stevenson, D., Amann, M., and Voss, M.: The global nitrogen cycle

in the twenty-first century, Philosophical transactions of the Royal Society of London. Series B, Biological sciences, 368, 20130 164, https://doi.org/10.1098/rstb.2013.0164, 2013.

Fowler, D., Steadman, C. E., Stevenson, D., Coyle, M., Rees, R. M., Skiba, U. M., Sutton, M. A., Cape, J. N., Dore, A. J., Vieno, M., Simpson, D., Zaehle, S., Stocker, B. D., Rinaldi, M., Facchini, M. C., Flechard, C. R., Nemitz, E., Twigg, M., Erisman, J. W., Butterbach-Bahl, K., and Galloway, J. N.: Effects of global change during the 21st century on the nitrogen cycle, Atmospheric Chemistry and Physics, 15, 13 849–13 893, https://doi.org/10.5194/acp-15-13849-2015, 2015.

Ge, X., Wexler, A. S., and Clegg, S. L.: Atmospheric amines – Part I. A review, Atmospheric Environment, 45, 524–546, https://doi.org/10.1016/j.atmosenv.2010.10.012, http://www.sciencedirect.com/science/article/pii/S1352231010008745, 2011.

Gibb, S. W., Mantoura, R. F. C., and Liss, P. S.: Ocean-atmosphere exchange and atmospheric speciation of ammonia and methylamines in the region of the NW Arabian Sea, Global Biogeochemical Cycles, 13, 161–178, https://doi.org/10.1029/98GB00743, 1999.

Graus, M., Müller, M., and Hansel, A.: High resolution PTR-TOF: quantification and formula confirmation of VOC in real time, Journal of the American Society for Mass Spectrometry, 21, 1037–1044, https://doi.org/10.1016/j.jasms.2010.02.006, 2010.

Hoffmann, E. H., Tilgner, A., Schrödner, R., Bräuer, P., Wolke, R., and Herrmann, H.: An advanced modeling study on the impacts and atmospheric implications of multiphase dimethyl sulfide chemistry, Proceedings of the National Academy of Sciences of the United States of America, 113, 11 776–11 781, https://doi.org/10.1073/pnas.1606320113, 2016.

Jackson, T., Chuprin, A., Sathyendranath, S., Grant, M., Zühlke, M., Dingle, J., Storm, T., Boettcher, M., and Fomferra, N.: Ocean Colour Climate Change Initiative: version 4.0, ftp://ftp.rsg.pml.ac.uk/occci-v4.0/geographic/netcdf/8day/chlor_a/2017/, 2019.

Johnson, M. T., Liss, P. S., Bell, T. G., Lesworth, T. J., Baker, A. R., Hind, A. J., Jickells, T. D., Biswas, K. F., Woodward, E. M. S., and Gibb, S. W.: Field observations of the ocean-atmosphere exchange of ammonia: Fundamental importance of temperature as revealed by a comparison of high and low latitudes, Global Biogeochemical Cycles, 22, n/a–n/a, https://doi.org/10.1029/2007GB003039, 2008.

Jordan, A., Haidacher, S., Hanel, G., Hartungen, E., Märk, L., Seehauser, H., Schottkowsky, R., Sulzer, P., and Märk, T. D.: A high resolution and high sensitivity proton-transfer-reaction time-of-flight mass spectrometer (PTR-TOF-MS), International Journal of Mass Spectrometry, 286, 122–128, https://doi.org/10.1016/j.ijms.2009.07.005, 2009.

Junttila, M. H. and Hormi, O. O. E.: Methanesulfonamide: a cosolvent and a general acid catalyst in sharpless asymmetric dihydroxylations, The Journal of organic chemistry, 74, 3038–3047, https://doi.org/10.1021/jo8026998, 2009.

Kämpf, J. and Chapman, P.: Upwelling Systems of the World, Springer International Publishing, Cham, https://doi.org/10.1007/978-3-319-42524-5, 2016.

Khan, M., Gillespie, S., Razis, B., Xiao, P., Davies-Coleman, M. T., Percival, C. J., Derwent, R. G., Dyke, J. M., Ghosh, M. V., Lee, E., and Shallcross, D. E.: A modelling study of the atmospheric chemistry of DMS using the global model, STOCHEM-CRI, Atmospheric Environment, 127, 69–79, https://doi.org/10.1016/j.atmosenv.2015.12.028, 2016.

Kiene, R. P., Linn, L. J., and Bruton, J. A.: New and important roles for DMSP in marine microbial communities, Journal of Sea Research, 43, 209–224, https://doi.org/10.1016/S1385-1101(00)00023-X, 2000.

Kloster, S., Feichter, J., Maier-Reimer, E., Six, K. D., Stier, P., and Wetzel, P.: DMS cycle in the marine ocean-atmosphere system – a global model study, Biogeosciences, 3, 29–51, https://pure.mpg.de/pubman/item/item_994660_3/component/file_994659/Biogeosci_3-29.pdf, 2006.

Kukui, A., Borissenko, D., Laverdet, G., and Le Bras, G.: Gas-Phase Reactions of OH Radicals with Dimethyl Sulfoxide and Methane Sulfinic Acid Using Turbulent Flow Reactor and Chemical Ionization Mass Spectrometry, The Journal of Physical Chemistry A, 107, 5732–5742, https://doi.org/10.1021/jp0276911, 2003.

Kulmala, M., Petäjä, T., Ehn, M., Thornton, J., Sipilä, M., Worsnop, D. R., and Kerminen, V.-M.: Chemistry of atmospheric nucleation: on the recent advances on precursor characterization and atmospheric cluster composition in connection with atmospheric new particle formation, Annual review of physical chemistry, 65, 21–37, https://doi.org/10.1146/annurev-physchem-040412-110014, 2014.

Lai, S. C., Williams, J., Arnold, S. R., Atlas, E. L., Gebhardt, S., and Hoffmann, T.: Iodine containing species in the remote marine boundary layer: A link to oceanic phytoplankton, Geophysical Research Letters, 38, n/a–n/a, https://doi.org/10.1029/2011GL049035, 2011.

Lana, A., Bell, T. G., Simó, R., Vallina, S. M., Ballabrera-Poy, J., Kettle, A. J., Dachs, J., Bopp, L., Saltzman, E. S., Stefels, J., Johnson, J. E., and Liss, P. S.: An updated climatology of surface dimethlysulfide concentrations and emission fluxes in the global ocean, Global Biogeochemical Cycles, 25, n/a–n/a, https://doi.org/10.1029/2010GB003850, 2011.

Li, H., Zhang, X., Zhong, J., Liu, L., Zhang, H., Chen, F., Li, Z., Li, Q., and Ge, M.: The role of hydroxymethanesulfonic acid in the initial stage of new particle formation, Atmospheric Environment, 189, 244–251, https://doi.org/10.1016/j.atmosenv.2018.07.003, http://www.sciencedirect.com/science/article/pii/S1352231018304424, 2018.

Lindinger, W., Hansel, A., and Jordan, A.: On-line monitoring of volatile organic compounds at pptv levels by means of proton-transfer-reaction mass spectrometry (PTR-MS) medical applications, food control and environmental research, International Journal of Mass Spectrometry and Ion Processes, 173, 191–241, https://doi.org/10.1016/S0168-1176(97)00281-4, 1998.

Liss, P. S. and Slater, P. G.: Flux of Gases across the Air-Sea Interface, Nature, 247, 181–184, https://doi.org/10.1038/247181a0, https://www.nature.com/articles/247181a0.pdf, 1974.

Liss, P. S., Marandino, C. A., Dahl, E. E., Helmig, D., Hintsa, E. J., Hughes, C., Johnson, M. T., Moore, R. M., Plane, J. M. C., Quack, B., Singh, H. B., Stefels, J., von Glasow, R., and Williams, J.: Short-Lived Trace Gases in the Surface Ocean and the Atmosphere, in: Ocean-Atmosphere Interactions of Gases and Particles, edited by Liss, P. and Johnson, M. T., Springer Earth System Sciences, pp. 1–54, Springer-Verlag GmbH, [Erscheinungsort nicht ermittelbar], https://doi.org/10.1007/978-3-642-25643-1_1, https://doi.org/10.1007/978-3-642-25643-1_1, 2014.

Liu, X., Deming, B., Pagonis, D., Day, D. A., Palm, B. B., Talukdar, R., Roberts, J. M., Veres, P. R., Krechmer, J. E., Thornton, J. A., de Gouw, J. A., Ziemann, P. J., and Jimenez, J. L.: Effects of gas–wall interactions on measurements of semivolatile compounds and small polar molecules, Atmospheric Measurement Techniques, 12, 3137–3149, https://doi.org/10.5194/amt-12-3137-2019, https://www.atmos-meas-tech.net/12/3137/2019/amt-12-3137-2019.pdf, 2019.

Mardyukov, A. and Schreiner, P. R.: Atmospherically Relevant Radicals Derived from the Oxidation of Dimethyl Sulfide, Accounts of chemical research, 51, 475–483, https://doi.org/10.1021/acs.accounts.7b00536, 2018.

Pagonis, D., Krechmer, J. E., de Gouw, J., Jimenez, J. L., and Ziemann, P. J.: Effects of gas–wall partitioning in Teflon tubing and instrumentation on time-resolved measurements of gas-phase organic compounds, Atmospheric measurement techniques, 10, 4687–4696, https://doi.org/10.5194/amt-10-4687-2017, https://www.atmos-meas-tech.net/10/4687/2017/amt-10-4687-2017.pdf, 2017.

Paulot, F., Jacob, D. J., Johnson, M. T., Bell, T. G., Baker, A. R., Keene, W. C., Lima, I. D., Doney, S. C., and Stock, C. A.: Global oceanic emission of ammonia: Constraints from seawater and atmospheric observations, Global Biogeochemical Cycles, 29, 1165–1178, https://doi.org/10.1002/2015GB005106, 2015.

Pfannerstill, E. Y., Wang, N., Edtbauer, A., Bourtsoukidis, E., Crowley, J. N., Dienhart, D., Eger, P. G., Ernle, L., Fischer, H., Hottmann, B., Paris, J.-D., Stönner, C., Tadic, I., Walter, D., Lelieveld, J., and Williams, J.: Shipborne measurements of total OH reactivity around the Arabian Peninsula and its role in ozone chemistry, Atmospheric Chemistry and Physics Discussions, pp. 1–38, https://doi.org/10.5194/acp-2019-416, https://www.atmos-chem-phys-discuss.net/acp-2019-416/acp-2019-416.pdf, 2019.

Platt, U. and Hönninger, G.: The role of halogen species in the troposphere, Chemosphere, 52, 325–338, https://doi.org/10.1016/S0045-6535(03)00216-9, http://www.sciencedirect.com/science/article/pii/S0045653503002169, 2003.

Prinn, R. G., Huang, J., Weiss, R. F., Cunnold, D. M., Fraser, P. J., Simmonds, P. G., McCulloch, A., Harth, C., Reimann, S., Salameh, P., O'Doherty, S., Wang, R. H. J., Porter, L. W., Miller, B. R., and Krummel, P. B.: Evidence for variability of atmospheric hydroxyl radicals over the past quarter century, Geophysical Research Letters, 32, https://doi.org/10.1029/2004GL022228, https://agupubs.onlinelibrary.wiley.com/doi/pdf/10.1029/2004GL022228, 2005.

Quinn, P. K. and Bates, T. S.: The case against climate regulation via oceanic phytoplankton sulphur emissions, Nature, 480, 51–56, https://doi.org/10.1038/nature10580, 2011.

Read, K. A., Mahajan, A. S., Carpenter, L. J., Evans, M. J., Faria, B. V. E., Heard, D. E., Hopkins, J. R., Lee, J. D., Moller, S. J., Lewis, A. C., Mendes, L., McQuaid, J. B., Oetjen, H., Saiz-Lopez, A., Pilling, M. J., and Plane, J. M. C.: Extensive halogen-mediated ozone destruction over the tropical Atlantic Ocean, Nature, 453, 1232–1235, https://doi.org/10.1038/nature07035, https://www.nature.com/articles/nature07035.pdf, 2008.

Schwartz, S. E.: Factors Governing Dry Deposition of Gases to Surface-Water, in: PRECIPITATION SCAVENGING AND ATMOSPHERE-SURFACE EXCHANGE, VOLS 1-3, edited by Schwartz, S. E. and SLINN, W. G., pp. 789–801, HEMISPHERE PUBL CORP, NEW YORK, 1992.

Sciare, J., Kanakidou, M., and Mihalopoulos, N.: Diurnal and seasonal variation of atmospheric dimethylsulfoxide at Amsterdam Island in the southern Indian Ocean, JOURNAL OF GEOPHYSICAL RESEARCH,, pp. 17 257–17 265, 2000.

Sievert, S., Kiene, R., and Schulz-Vogt, H.: The Sulfur Cycle, Oceanography, 20, 117–123, https://doi.org/10.5670/oceanog.2007.55, 2007.

Sipilä, M., Berndt, T., Petäjä, T., Brus, D., Vanhanen, J., Stratmann, F., Patokoski, J., Mauldin, R. L., Hyvärinen, A.-P., Lihavainen, H., and Kulmala, M.: The Role of Sulfuric Acid in Atmospheric Nucleation, Science, 327, 1243–1246, https://doi.org/10.1126/science.1180315, https://science.sciencemag.org/content/sci/327/5970/1243.full.pdf, 2010.

Sköld, O.: Sulfonamides and trimethoprim, Expert review of anti-infective therapy, 8, 1–6, https://doi.org/10.1586/eri.09.117, 2010.

Su, T. and Chesnavich, W. J.: Parametrization of the ion–polar molecule collision rate constant by trajectory calculations, The Journal of Chemical Physics, 76, 5183–5185, https://doi.org/10.1063/1.442828, 1982.

Turnipseed, A. A., Barone, S. B., and Ravishankara, A. R.: Reaction of OH with Dimethyl Sulfide. 2. Products and Mechanisms, The Journal of Physical Chemistry, 100, 14 703–14 713, https://doi.org/10.1021/jp960867c, 1996.

Veres, P. R., Faber, P., Drewnick, F., Lelieveld, J., and Williams, J.: Anthropogenic sources of VOC in a football stadium: Assessing human emissions in the atmosphere, Atmospheric Environment, 77, 1052–1059, https://doi.org/10.1016/j.atmosenv.2013.05.076, 2013.

Vila-Costa, M., Simó, R., Harada, H., Gasol, J. M., Slezak, D., and Kiene, R. P.: Dimethylsulfoniopropionate uptake by marine phytoplankton, Science (New York, N.Y.), 314, 652–654, https://doi.org/10.1126/science.1131043, 2006.

Voss, M., Bange, H. W., Dippner, J. W., Middelburg, J. J., Montoya, J. P., and Ward, B.: The marine nitrogen cycle: recent discoveries, uncertainties and the potential relevance of climate change, Philosophical transactions of the Royal Society of London. Series B, Biological sciences, 368, 20130 121, https://doi.org/10.1098/rstb.2013.0121, 2013.

Wang, N., Edtbauer, A., Stönner, C., Pozzer, A., Bourtsoukidis, E., Ernle, L., Dienhart, D., Hottmann, B., Fischer, H., Schuladen, J., Crowley, J. N., Paris, J.-D., Lelieveld, J., and Williams, J.: Measurements of carbonyl compounds around the Arabian Peninsula indicate large missing sources of acetaldehyde, Atmospheric Chemistry and Physics Discussions, https://doi.org/10.5194/acp-2020-135, 2020.

Warneke, C. and de Gouw, J. A.: Organic trace gas composition of the marine boundary layer over the northwest Indian Ocean in April 2000, Atmospheric Environment, 35, 5923–5933, https://doi.org/10.1016/S1352-2310(01)00384-3, 2001.

Webb, A. L., van Leeuwe, M. A., den Os, D., Meredith, M. P., J Venables, H., and Stefels, J.: Extreme spikes in DMS flux double estimates of biogenic sulfur export from the Antarctic coastal zone to the atmosphere, Scientific reports, 9, 2233, https://doi.org/10.1038/s41598-019-38714-4, 2019.

Weber, R. J., MARTI, J. J., McMURRY, P. H., Eisele, F. L., Tanner, D. J., and Jefferson, A.: MEASURED ATMOSPHERIC NEW PARTICLE FORMATION RATES: IMPLICATIONS FOR NUCLEATION MECHANISMS, Chemical Engineering Communications, 151, 53–64, https://doi.org/10.1080/00986449608936541, 1996.

Weber, R. J., Chen, G., Davis, D. D., Mauldin, R. L., Tanner, D. J., Eisele, F. L., Clarke, A. D., Thornton, D. C., and Bandy, A. R.: Measurements of enhanced H2SO4 and 3–4 nm particles near a frontal cloud during the First Aerosol Characterization Experiment (ACE 1), Journal of Geophysical Research: Atmospheres, 106, 24 107–24 117, https://doi.org/10.1029/2000JD000109, https://agupubs.onlinelibrary.wiley.com/doi/full/10.1029/2000JD000109, 2001.

Xie, H.-B., Elm, J., Halonen, R., Myllys, N., Kurtén, T., Kulmala, M., and Vehkamäki, H.: Atmospheric Fate of Monoethanolamine: Enhancing New Particle Formation of Sulfuric Acid as an Important Removal Process, Environmental science & technology, 51, 8422–8431, https://doi.org/10.1021/acs.est.7b02294, 2017.

Yang, M., Beale, R., Liss, P., Johnson, M., Blomquist, B., and Nightingale, P.: Air–sea fluxes of oxygenated volatile organic compounds across the Atlantic Ocean, Atmospheric Chemistry and Physics, 14, 7499–7517, https://doi.org/10.5194/acp-14-7499-2014, https://www.atmos-chem-phys.net/14/7499/2014/acp-14-7499-2014.pdf, 2014.

Yassaa, N., Peeken, I., Zöllner, E., Bluhm, K., Arnold, S., Spracklen, D., and Williams, J.: Evidence for marine production of monoterpenes, Environmental Chemistry, 5, 391, https://doi.org/10.1071/EN08047, 2008.

Zavarsky, A., Booge, D., Fiehn, A., Krüger, K., Atlas, E., and Marandino, C.: The Influence of Air-Sea Fluxes on Atmospheric Aerosols During the Summer Monsoon Over the Tropical Indian Ocean, Geophysical Research Letters, 45, 418–426, https://doi.org/10.1002/2017GL076410, 2018.

Supplement

1 Deposition lifetime

The exchange flux F of various gases between an air and water interface can be predicted with the help of a two-layer model [5, 9, 10]:

$$F = K_G(G - \frac{A}{H}). \tag{1}$$

Where K_G is the overall mass-transfer coefficient (has dimensions of velocity), G is the gas phase concentration, A the aqueous phase concentration and H the Henry's law constant in the dimensionless form. If we assume that the aqueous phase concentration is zero (e.g. outside of the Somalia upwelling when traveling towards the ship) then equation 1 simplifies to:

$$F = K_G G. \tag{2}$$

The mass-transfer coefficient K_G can be expressed as:

$$\frac{1}{K_G} = \frac{1}{k_G} + \frac{1}{\frac{1}{4}\nu\alpha} + \frac{1}{Hk_L\beta}. \tag{3}$$

In this equation k_G is the gas phase and k_L the liquid phase mass-transfer coefficient, ν the mean molecular speed of the molecule, α the mass-accommodation coefficient and β an enhancement coefficient of the aqueous phase mass transfer flux due to removal of the molecule by chemical reactions. No enhancement means $\beta = 1$. The middle term which describes the interfacial resistance can be generally neglected in the natural environment because α is always sufficiently large [9]. If the molecule under investigation has a solubility of $H \gg H_{crit} = \frac{k_G}{k_L}$ then gas phase mass transport is dominant and the flux is independent of H. We determined a Henry's law constant in the range of $3.3 \times 10^4\,\mathrm{M\ atm^{-1}}$ - $6.5 \times 10^5\,\mathrm{M\ atm^{-1}}$ for methane sulfonamide (MSAM) (see Sect. S2) and for $DMSO_2$ literature indicates a value greater than $5 \times 10^4\,\mathrm{M\,atm^{-1}}$ [1]. This means that both are sufficiently soluble substances for which the assumption holds true that gas phase mass transport is controlling and the overall mass-transfer coefficient is given in the form:

$$\frac{1}{K_G} = \frac{1}{k_G}. \tag{4}$$

The gas phase mass-transfer coefficient for oceanic applications can be estimated with the help of the wind speed v [3]:

$$k_G = 0.0013v \tag{5}$$

for an observation height of 10 m which is the approximate height of observation during the AQABA campaign. The wind speed during the Arabian sea part in the second leg varied around $4\,\mathrm{m\ s^{-1}}$ and $14\,\mathrm{m\ s^{-1}}$ which yields: $K_G = 0.52\,\mathrm{cm\ s^{-1}}$ (v=$4\,\mathrm{m\ s^{-1}}$) and $K_G = 1.82\,\mathrm{cm\ s^{-1}}$ (v=$14\,\mathrm{m\ s^{-1}}$).
This in turn gives a lifetime (1/e) of 40 ± 14 hours for a wind speed of v=$4\,\mathrm{m\ s^{-1}}$ and about 11 ± 4 hours for v=$14\,\mathrm{m\ s^{-1}}$. The average marine boundary layer height used for the lifetime calculation was 750 ± 250 m.

2 Henry's law constant measurement

In order to resemble sea water more closely we added 35 g NaCl and 0.5 g $NaHCO_3$ to a combined volume of 1 L in MilliQ water. The obtained water is in the following referred to as sea water. Strictly speaking it does

not classify as artificial sea water because some ingredients like magnesium and calcium salts are missing. The MSAM mixing ratio of the headspace of 0.05 mol L^{-1} and 0.0005 mol L^{-1} MSAM in sea water, flushed with 100 ml min^{-1} of synthetic air (Air Liquide, Krefeld, Germany) each, was measured with a PTR-MS instrument. A range for the Henry's law constant was derived from these measurements as the ratio of the concentration of MSAM in solution (in M) vs. the measured partial pressure in the gas phase (in atm): 3.3×10^4 M atm^{-1} – 6.5×10^5 M atm^{-1}. Measurements were performed at 25° C and 995 mbar.

3 Weighting factors

Chlorophyll a water content encountered during transport of the airmasses towards the ship was weighted according to time before arrival at the ship. We employed a linear and an exponential weighting factor.

3.1 Linear weighting factors

The linear weighting factor is in the form $w = \frac{1}{1+p*t}$, where p is the weighting parameter and t is the number of hours before arrival at the ship's location. The *chlorophyll a* water content is multiplied by the weighting factor w to get the weighted *chlorophyll a* water content. We varied the p in the range from $p = 0.02$ to $p = 1$. The resulting plots are displayed in Fig. 1 till Fig. 4. A weighting parameter of $p = 0.02$ results in a high contribution and a $p = 1$ in a low contribution of *chlorophyll a* water content further away of the ship. Calculations of leg 1 with low weighting parameters $p = 0.02 - 0.1$ lead to a small increase in total *chlorophyll a* exposure of the trajectories (yellow lines in graphs) but no increase is seen when only the Somalia upwelling region is considered (black lines in graphs). This means that *chlorophyll a* pick up further away than the Somalia upwelling is responsible for this. MSAM and $DMSO_2$ are low or not detected during leg 1, therefore chlorophyll exposure in regions further away than the Somalia upwelling does not appear to play a role. The calculations in leg 2 are generally quite similar and therefore independent of the weighting parameter p.

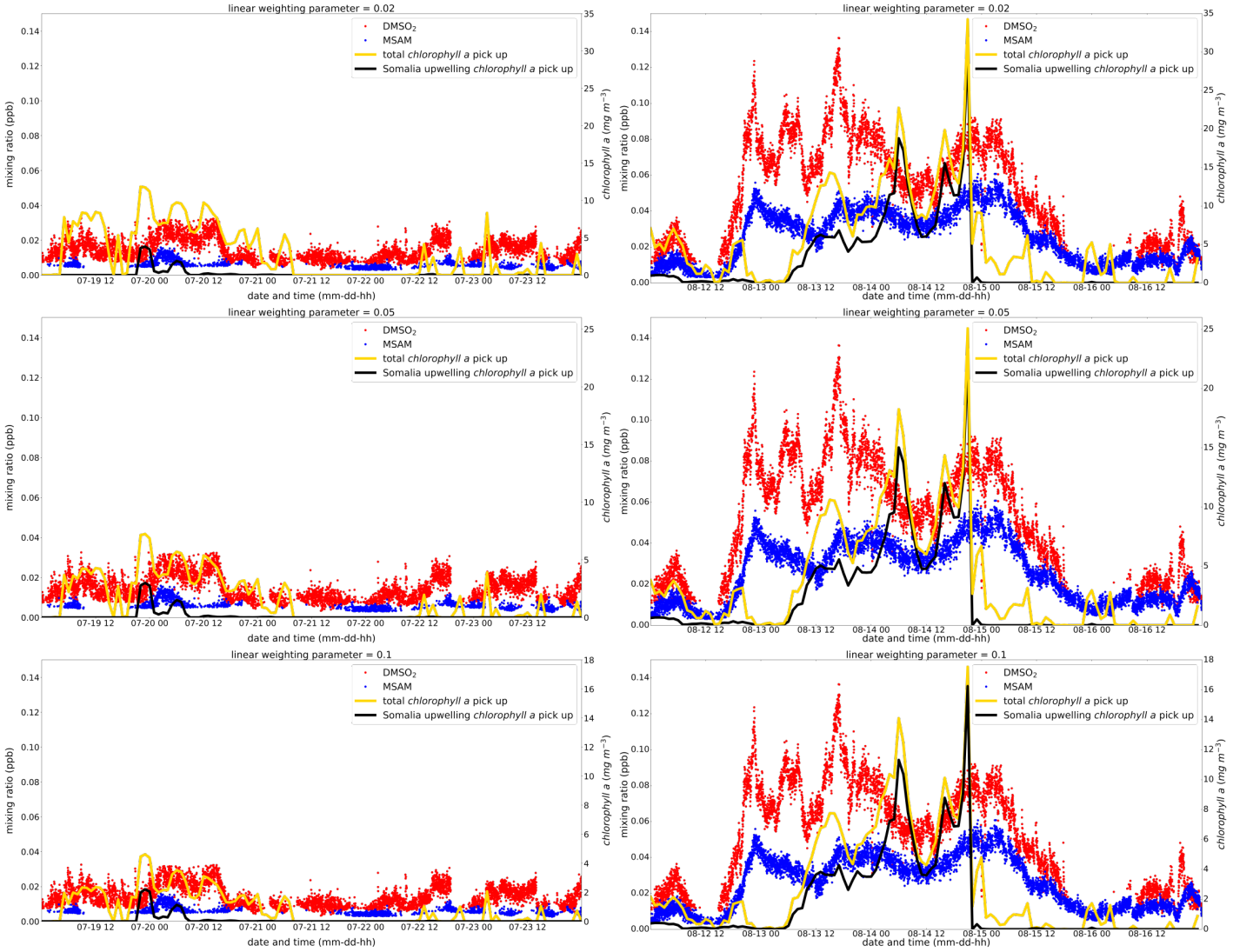

Figure 1: Linear weighting parameters from $p = 0.02 - 0.1$. The total *chlorophyll a* exposure (yellow line) and the *chlorophyll a* exposure originating from the Somalia upwelling region (black line) is plotted. The corresponding y-axis for the *chlorophyll a* exposure is displayed on the right side. Measured ambient mixing ratios in ppb for $DMSO_2$ and MSAM are plotted in red and blue with the corresponding y-axis on the left side. In the left column leg 1 and in the right column leg 2 is displayed.

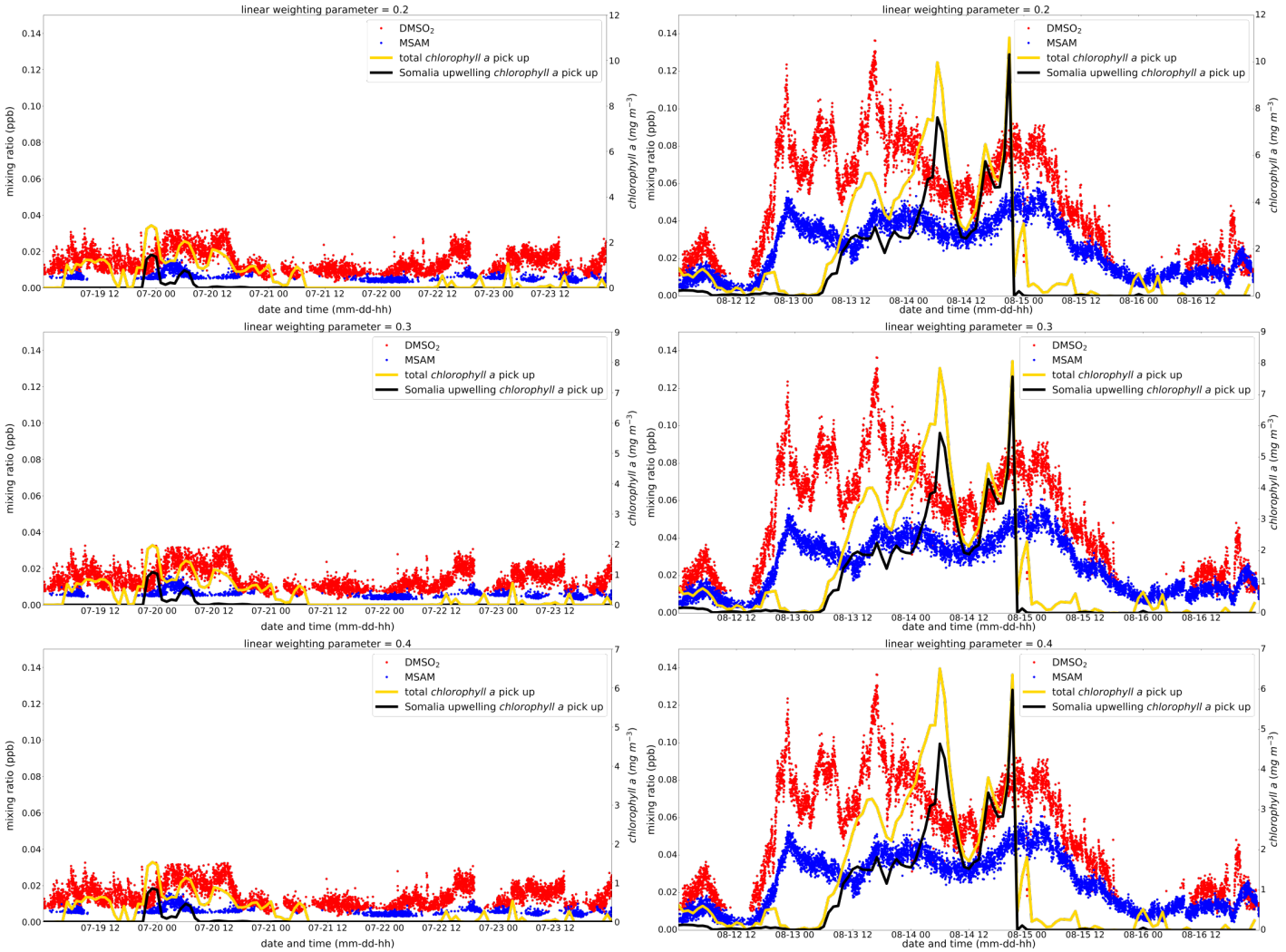

Figure 2: Linear weighting parameters from $p = 0.2 - 0.4$. The total *chlorophyll a* exposure (yellow line) and the *chlorophyll a* exposure originating from the Somalia upwelling region (black line) is plotted. The corresponding y-axis for the *chlorophyll a* exposure is displayed on the right side. Measured ambient mixing ratios in ppb for $DMSO_2$ and MSAM are plotted in red and blue with the corresponding y-axis on the left side. In the left column leg 1 and in the right column leg 2 is displayed.

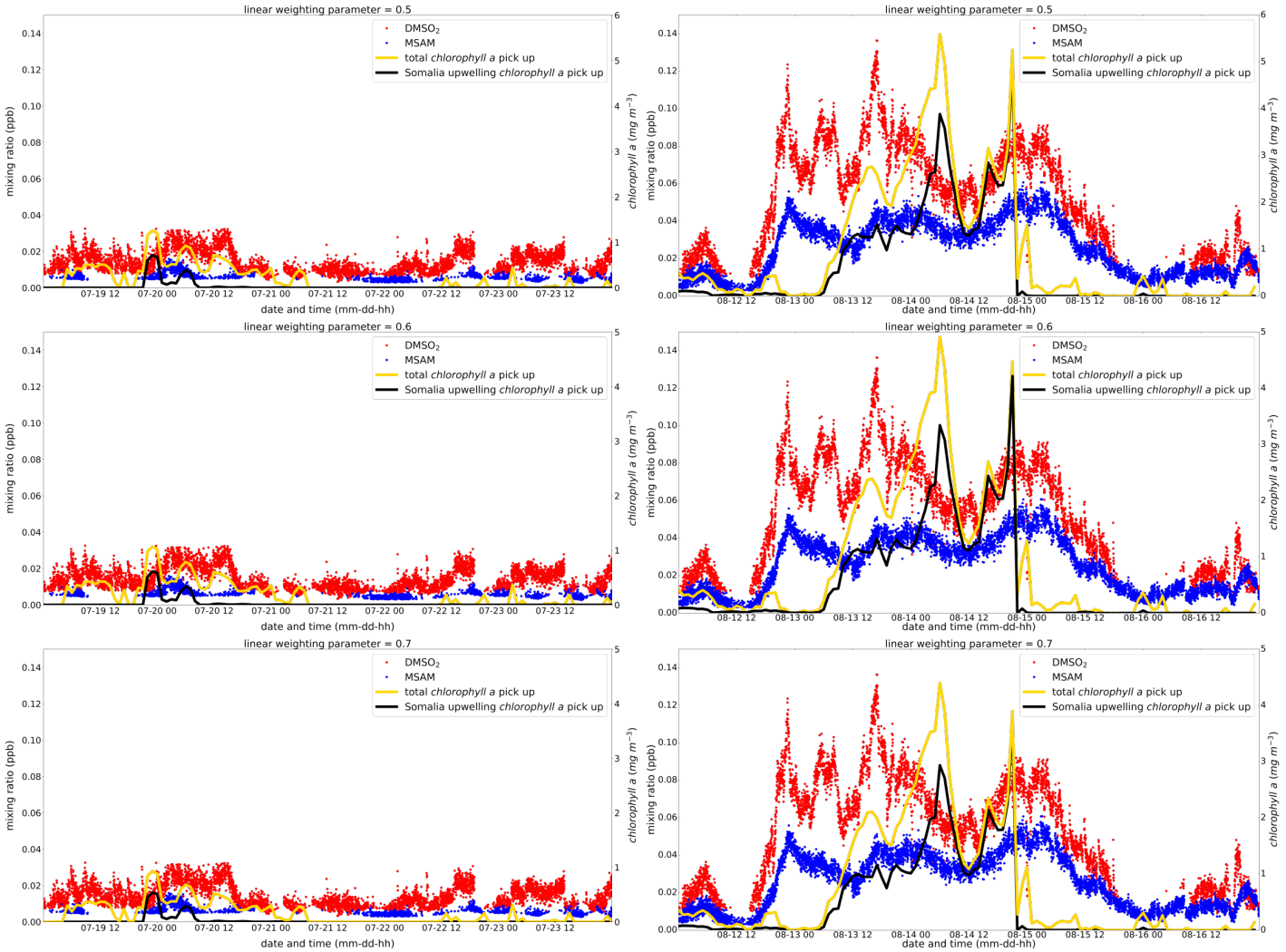

Figure 3: Linear weighting parameters from $p = 0.5 - 0.7$. The total *chlorophyll a* exposure (yellow line) and the *chlorophyll a* exposure originating from the Somalia upwelling region (black line) is plotted. The corresponding y-axis for the *chlorophyll a* exposure is displayed on the right side. Measured ambient mixing ratios in ppb for $DMSO_2$ and MSAM are plotted in red and blue with the corresponding y-axis on the left side. In the left column leg 1 and in the right column leg 2 is displayed.

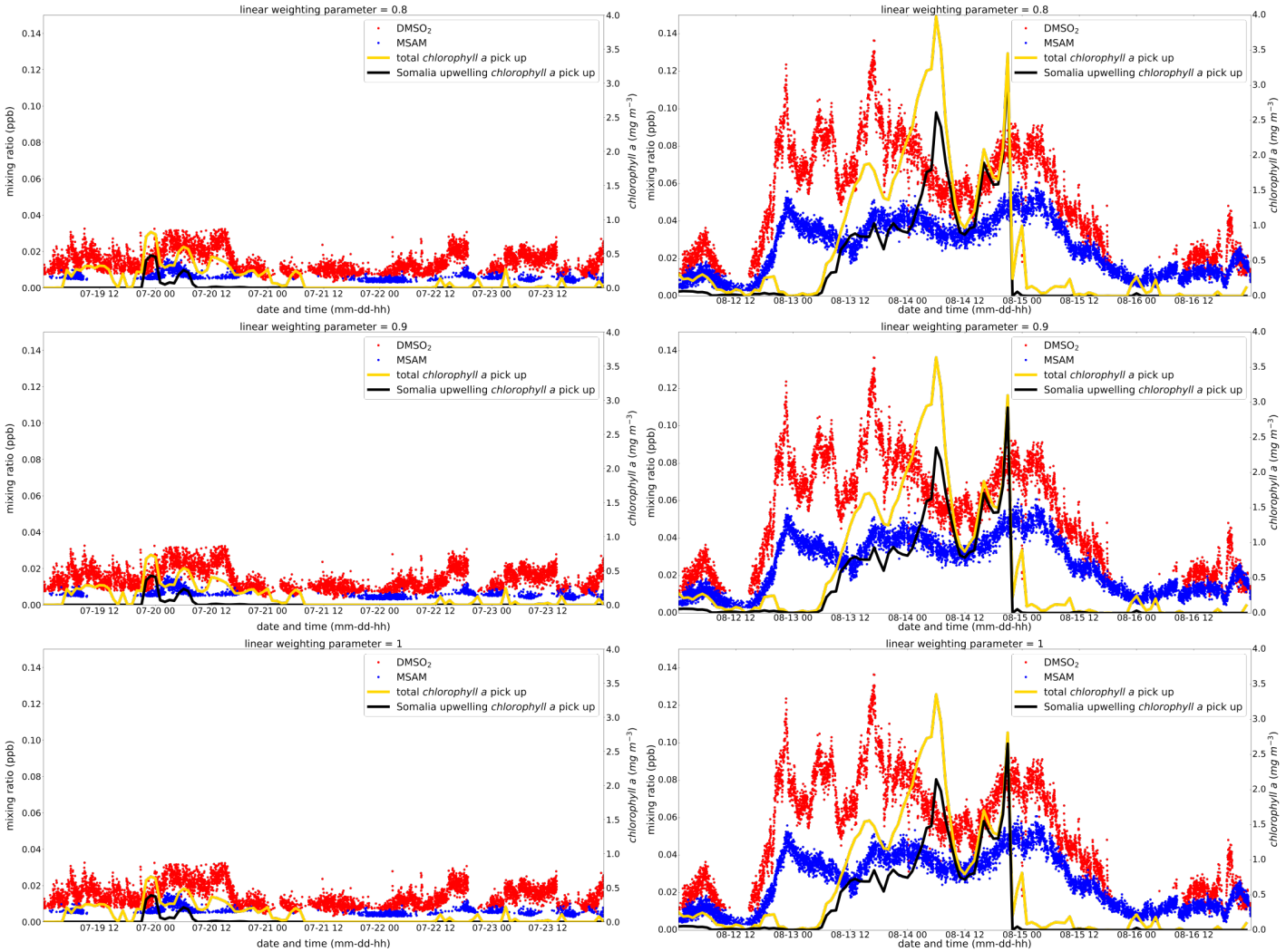

Figure 4: Linear weighting parameters from $p = 0.8 - 1$. The total *chlorophyll a* exposure (yellow line) and the *chlorophyll a* exposure originating from the Somalia upwelling region (black line) is plotted. The corresponding y-axis for the *chlorophyll a* exposure is displayed on the right side. Measured ambient mixing ratios in ppb for $DMSO_2$ and MSAM are plotted in red and blue with the corresponding y-axis on the left side. In the left column leg 1 and in the right column leg 2 is displayed.

3.2 Exponential weighting factors

The exponential weighting factor has the form $w_{exp} = p^t$, p, where p is the weighting parameter and t is the number of hours before arrival at the ship's location. The weighting factor is then multiplied with the respective *chlorophyll a* water content to yield the weighted *chlorophyll a*. The weighting parameter was varied from $p = 0.8$ to $p = 0.99$ (see Fig. 5 till Fig. 8). A weighting parameter of 1 means that all *chlorophyll a* water content is weighted equally. If p is close to 1 we see in the first leg a small increase in total *chlorophyll a* exposure coming from *chlorophyll a* pick up further away as the Somalia upwelling (as for the linear case). For the other cases we see in leg 2 that the Somalia upwelling region always constitutes the mayor part of the total *chlorophyll a* exposure, even in the case of $p = 0.8$, which discriminates strongly against chlorophyll exposure further away from the ship.

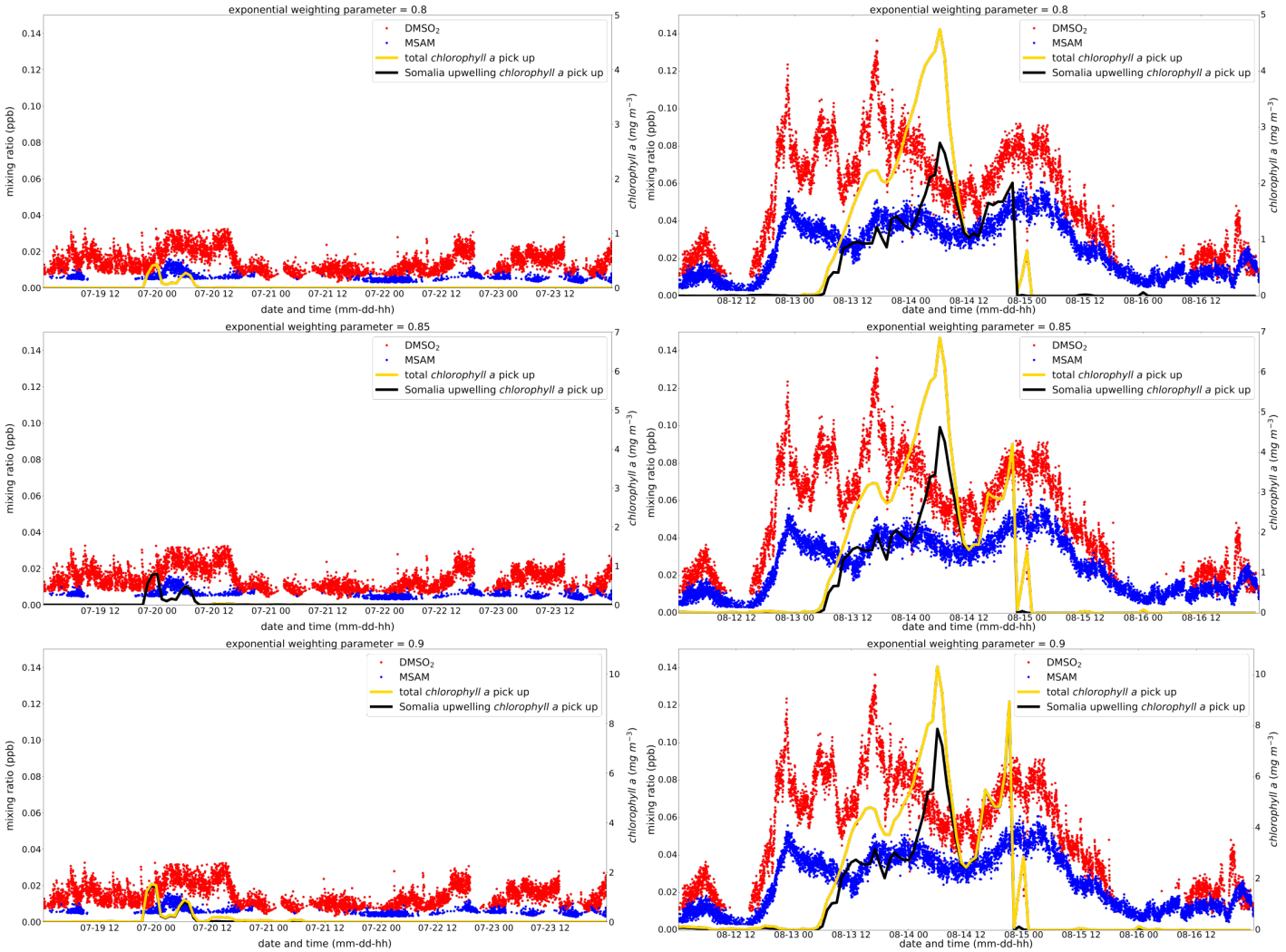

Figure 5: Exponential weighting parameters from $p = 0.8 - 0.9$. The total *chlorophyll a* exposure (yellow line) and the *chlorophyll a* exposure originating from the Somalia upwelling region (black line) is plotted. The corresponding y-axis for the *chlorophyll a* exposure is displayed on the right side. Measured ambient mixing ratios in ppb for $DMSO_2$ and MSAM are plotted in red and blue with the corresponding y-axis on the left side. In the left column leg 1 and in the right column leg 2 is displayed.

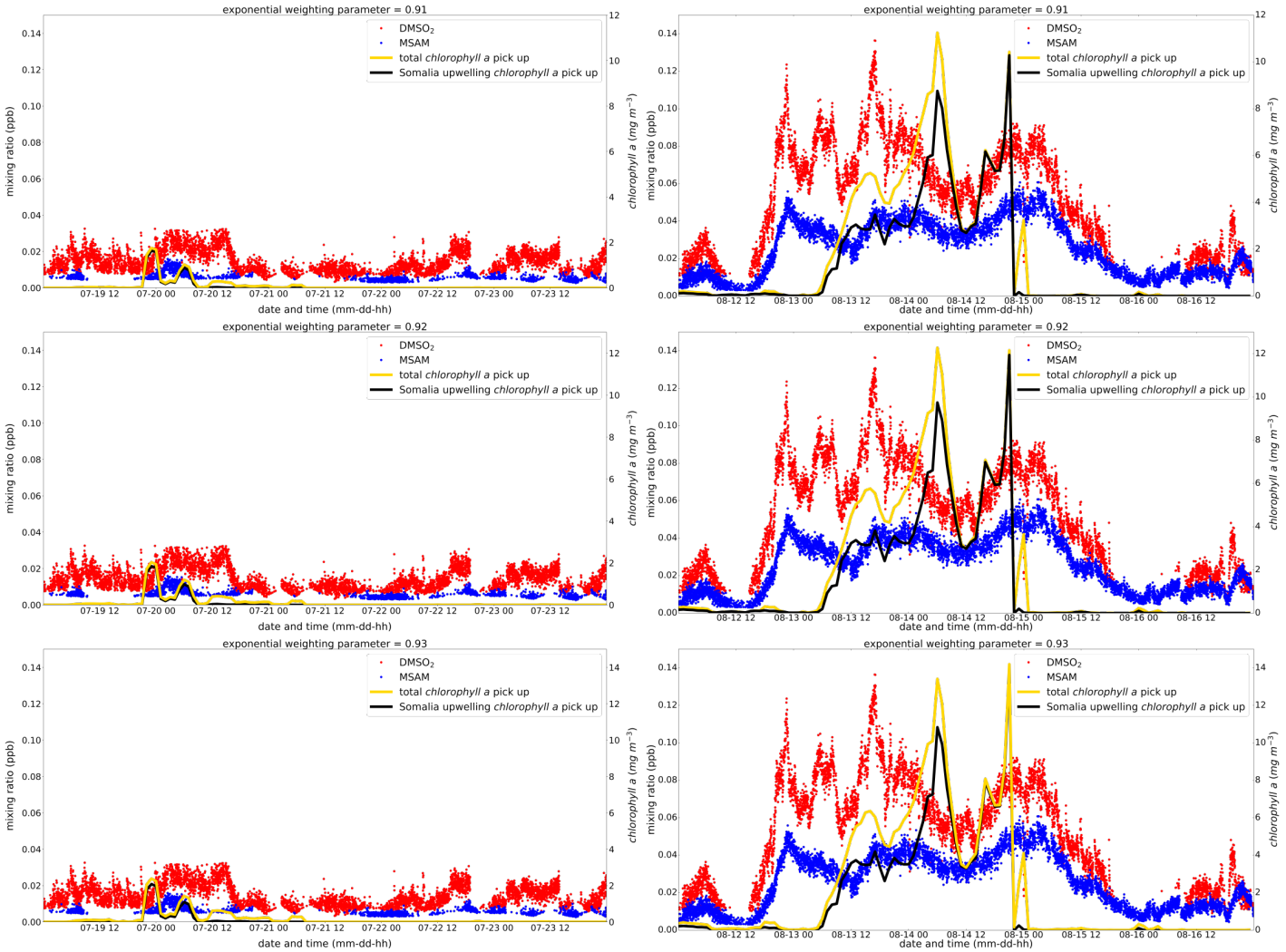

Figure 6: Exponential weighting parameters from $p = 0.91 - 0.93$. The total *chlorophyll a* exposure (yellow line) and the *chlorophyll a* exposure originating from the Somalia upwelling region (black line) is plotted. The corresponding y-axis for the *chlorophyll a* exposure is displayed on the right side. Measured ambient mixing ratios in ppb for $DMSO_2$ and MSAM are plotted in red and blue with the corresponding y-axis on the left side. In the left column leg 1 and in the right column leg 2 is displayed.

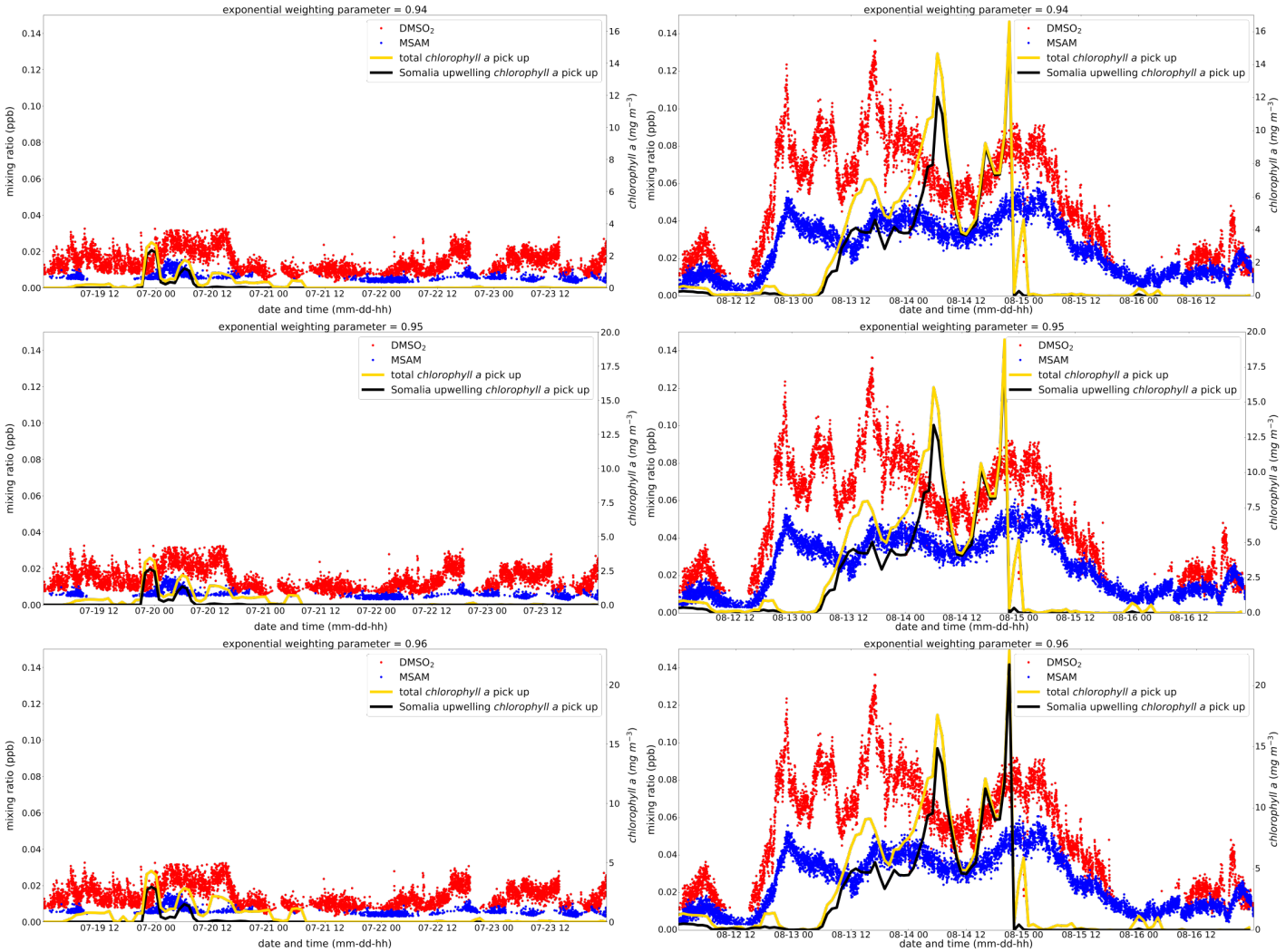

Figure 7: Exponential weighting parameters from $p = 0.94 - 0.96$. The total *chlorophyll a* exposure (yellow line) and the *chlorophyll a* exposure originating from the Somalia upwelling region (black line) is plotted. The corresponding y-axis for the *chlorophyll a* exposure is displayed on the right side. Measured ambient mixing ratios in ppb for $DMSO_2$ and MSAM are plotted in red and blue with the corresponding y-axis on the left side. In the left column leg 1 and in the right column leg 2 is displayed.

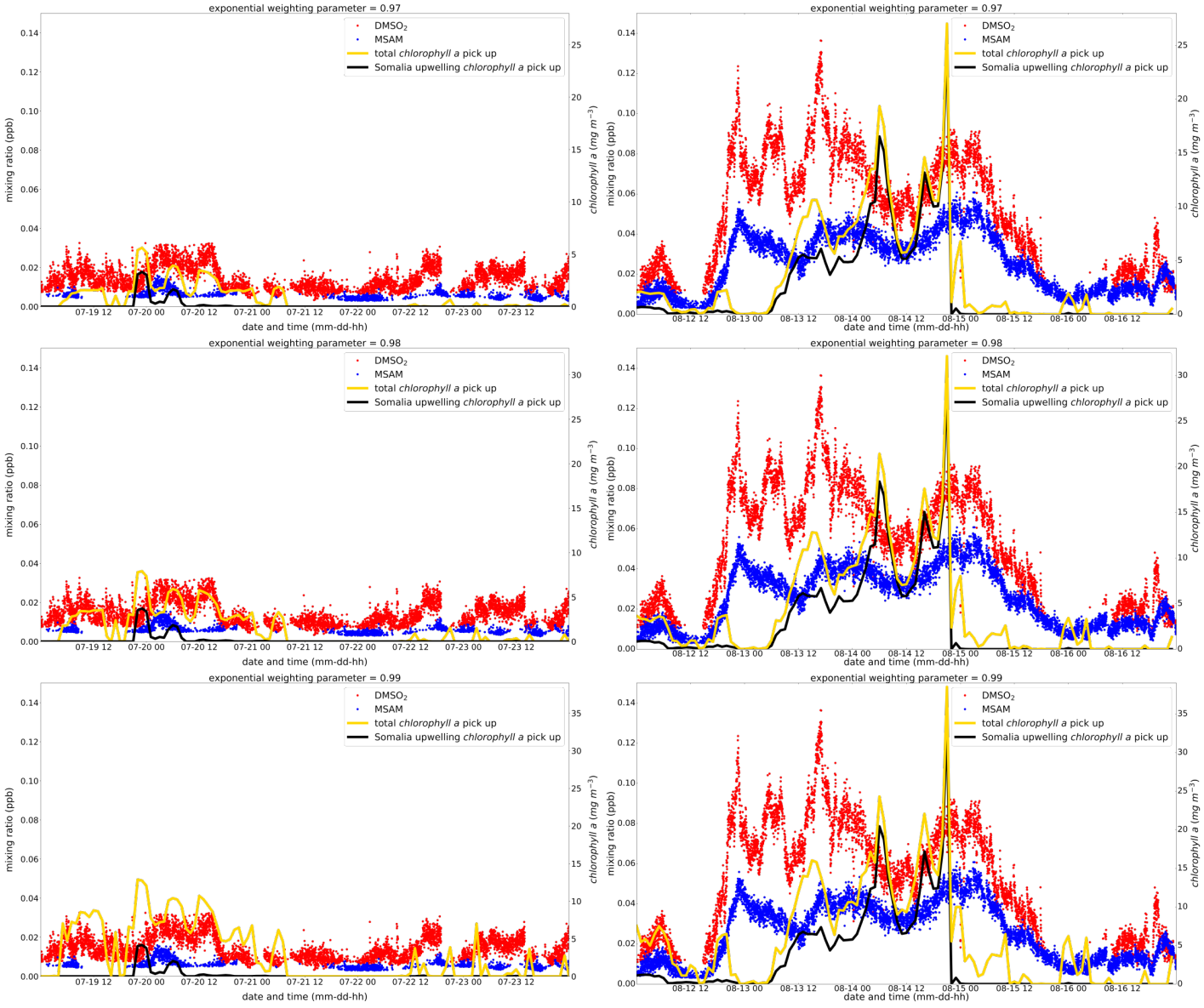

Figure 8: Exponential weighting parameters from $p = 0.97 - 0.99$. The total *chlorophyll a* exposure (yellow line) and the *chlorophyll a* exposure originating from the Somalia upwelling region (black line) is plotted. The corresponding y-axis for the *chlorophyll a* exposure is displayed on the right side. Measured ambient mixing ratios in ppb for $DMSO_2$ and MSAM are plotted in red and blue with the corresponding y-axis on the left side. In the left column leg 1 and in the right column leg 2 is displayed.

4 Diel variability plots

Diel variability of DMS, $DMSO_2$ and MSAM was calculated using only days when the wind was coming from the Somalia upwelling region. For whole days this only occurred on the 13th and 14th of August. On the 12th of August MSAM and $DMSO_2$ only started to increase and on the 15th they started to decline. The relatively short duration of the dataset available for diel variability calculations (2 days), taken on a moving platform means that variations can be interpreted as diel variations (driven by emission or atmospheric removal) or as source variations. Conclusions drawn from these plots should be treated with caution.

DMS seems to be higher at night than during the day (see Fig. 9 (a)). That is expected under stable conditions as DMS gets oxidized during daytime with OH.

$DMSO_2$ shows a tendency to be lower during daytime than at night (see Fig. 9 (b)). After sunset there is an increase in $DMSO_2$ which could hint at formation via NO_3 from the remaining DMSO concentrations.

MSAM we suggest is produced in the waters of the Somalia upwelling not in the atmosphere and subsequently transported to the ship. The time it took airmasses from the Somalia upwelling to reach the ship was 10 h to a day on the 13th and around 4 h on the 14th of August. So if we roughly assume an average travel time of 10 h for the diel cycle we have to shift the solar irradiation by 10 hours to the left (see orange filled curve in 9 (c)) in order to get the solar irradiation at the time of release from the Somalia upwelling. This hints at a production of MSAM in relation with photosynthetic activity since the higher values of MSAM occur together with higher solar irradiation in the Somalia upwelling region.

But as already stated above other effects like changes in transport time from the Somalia upwelling due to changes in wind speed and ship movement could have played a more important role.

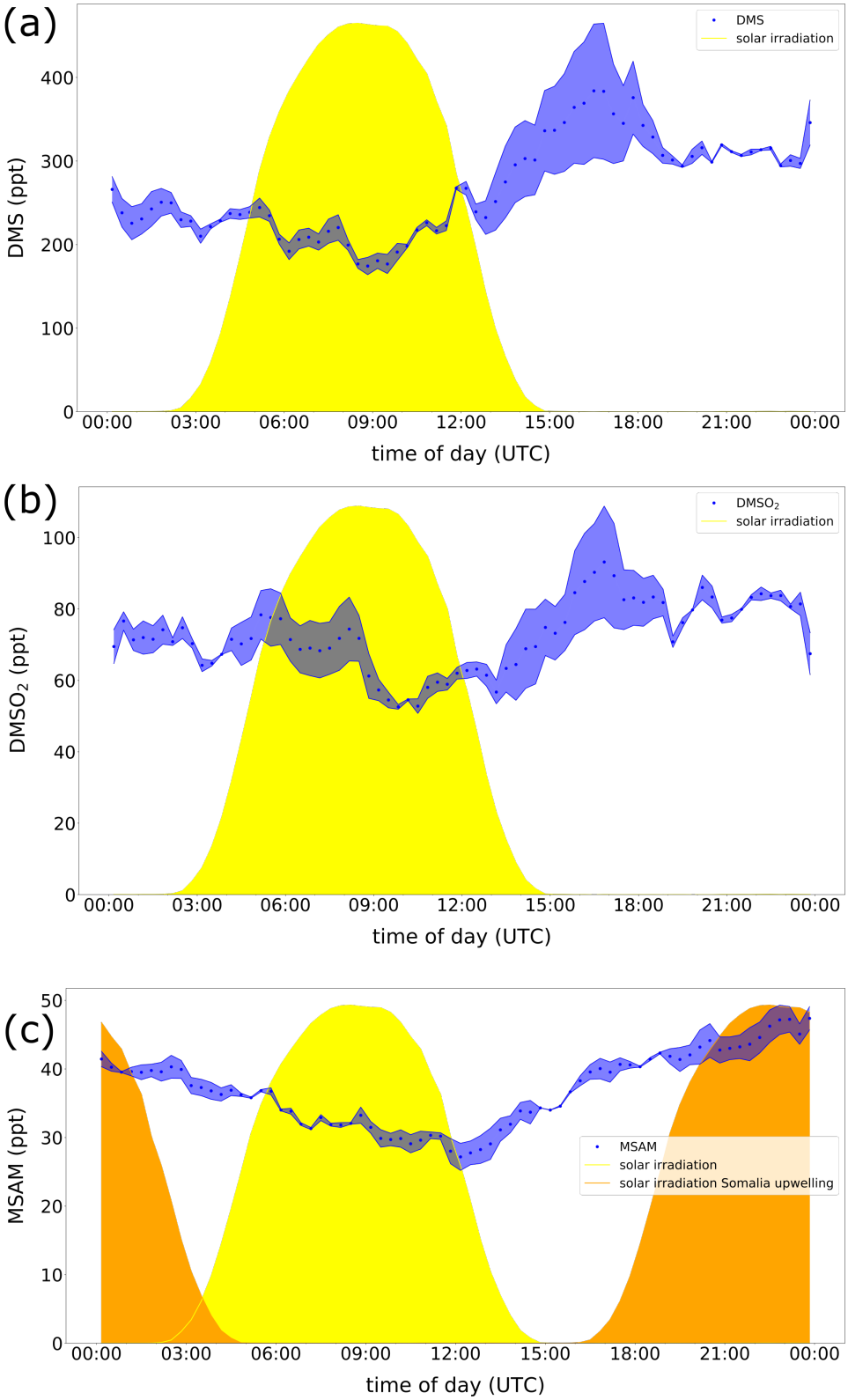

Figure 9: Diel variability of DMS (a), $DMSO_2$ (b) and MSAM (c). The blue dots are the mean and the light blue shading represents the 25th to 75th percentile. The yellow filled curve represents the solar irradiation. The diel variability was calculated using only days when the wind was coming the whole time from the Somalia upwelling region. Therefore we could only used the 13th and 14th of August for this calculations. The orange filled curve in (c) is the solar irradiation at the Somalia upwelling at the time of release of MSAM (assuming an average travel time of 10 h).

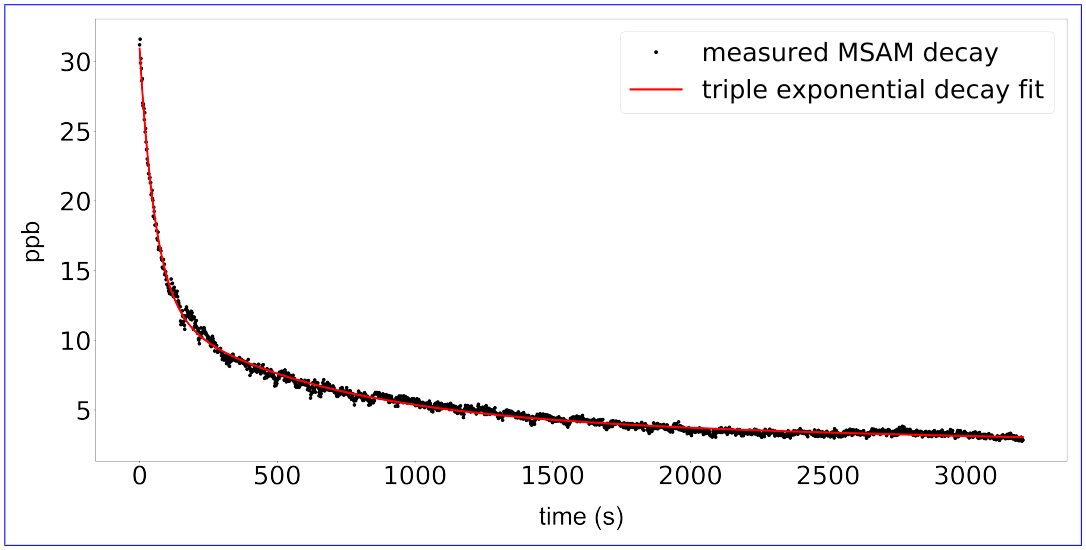

Figure 10: Measurement of the resulting time series of a step change in MSAM concentration. At $t = 0$ a 100 sccm flow of a stable MSAM concentration is replaced by clean zero air with the same humidity and flow. The resulting decay curve (black) is fitted with a triple exponential decay function (red).

5 Inlet characterization

We induced a concentration step change in order to determine the e-folding time (time it takes for a value to decay to 1/e) for an 1/8" teflon tubing inlet of 0.4 m length. An air flow of 100 sccm with a stable MSAM concentration was replaced by an air flow without MSAM (same flow and humidity). The resulting time series response (see Fig. 10) is an exponential decay which does not necessarily follow a single exponential decay [6] . A single exponential decay fit is not able to accurately fit the measured decay signal. We employed a triple exponential decay function to fit the signal $S(t)$ (see equation 6). In this equation the parameters a, b and c added together will give the concentration at $t = 0$ and the parameters τ_a, τ_b and τ_c are the decay timescales. The timescale τ gives the time it takes for the signal to drop to 1/e (e-folding time). The results of the fit yield $a = 18.3$, $b = 8.2$ and $c = 4.4$ (unit is ppb) with $\tau_a = 58$, $\tau_b = 581$ and $\tau_c = 8561$ (unit is seconds). This means that the observed exponential decay has different timescale regimes. First it decays quickly with a timescale of around one minute, then this increases to 10 minutes up to a timescale of around 142 minutes. To a good estimate the decay timescales depend proportionally on tubing length and diameter and inversely on the flow rate and saturation concentration [7]. On this basis we can estimate the decay timescales of our AQABA inlet setup (length 10 m, 1/2" Teflon tubing, flow of 3 slpm) to 3.3 minutes, 33 minutes and 8 hours. Therefore concentration changes happening even on timescales of half an hour or longer will be smoothed, i.e. the real variance of the concentration might have been considerably larger.

$$S(t) = a * e^{-\frac{t}{\tau_a}} + b * e^{-\frac{t}{\tau_b}} + c * e^{-\frac{t}{\tau_c}} \tag{6}$$

6 Synthesis of MSAM

The partitioning of MSAM to the inside wall of the Teflon tubing raises the question whether the observed MSAM could be generated there on surfaces. No inlet test was done during the campaign to address this issue since this discovery was a surprise. Therefore, we cannot rule out that such an effect occurs. However we do consider it unlikely that MSAM was formed via a surface reaction of $DMSO_2$ (or an analogous species) with NH_3 or NH_4^+ . $DMSO_2$ as well as NH_3 and NH_4^+ are both very unreactive molecules. Additionally, we see no way of how NH_4^+ and NH_3 could lose their hydrogen atoms in order to form the requisite NH_2 group. A

chemical synthesis pathway for sulfonamides from sulfonic acids has been published [2]. The first step towards the production of MSAM would be removal of the whole OH group of methane sulfonic acid (MSA), creating a $CH_3SO_2^+$ ion. In an aqueous solution, the preferred reaction is, however, the removal of H^+, i.e. forming $CH_3SO_3^-$.
In this chemical synthesis, aggressive reagents such as trichlorotriazine and high energy (e.g. from a microwave) are used to create an intermediate CH_3SO_2Cl which reacts as a $CH_3SO_2^+$ ion. In the second step, this $CH_3SO_2^+$ ion reacts with an amine (for MSAM formation this would need to be replaced by NH_3) in a strong basic solution (NaOH(aq)), abstracting an H from NH_3 to form MSAM. The fact that sulfonic acids and not sulfones are used as precursors in synthesis of sulfonamides points out that formation from sulfones is either not possible or more difficult than with sulfonic acids. Formation of MSAM therefore needs aggressive reagents, input of energy and strong basic conditions which were not present in our inlet. We are not aware of any other possible pathways which could form MSAM in our inlet. However we cannot rule it out completely, thus it remains a uncertainty that future studies should clarify.

7 MSAM concentration in seawater

We cannot provide an accurate calculation for the waterside concentration required as the physical conditions in the Somalia upwelling region are not known and the Henry's law constant is uncertain. Calculation of the water concentration needed to support measured atmospheric concentrations of MSAM would require a model. Due to the lack of knowledge of the conditions at the upwelling region we consider that not feasible.
However from equation 1 we can calculate the minimum MSAM water concentration (A) required to produce a positive flux to the atmosphere at a given atmospheric concentration (G). Due to the high Henry's law constant (H) compared e.g. to DMS it has to be expected that, with this two-layer model, MSAM water concentrations have to be considerably larger than DMS water concentrations in order to produce a flux to the atmosphere. Concentrations higher than $A = G * H$ will result in a flux to the atmosphere. The water side concentration (for G =50 ppt and $H = 3.3 \times 10^4$ M atm^{-1}) needs to be higher than 1700 nM. This appears very high in comparison with previously reported water phase concentration of VOC [8, 4]. Measurements of water concentrations together with ambient air measurements of MSAM in an upwelling region are needed to better understand the ocean air exchange of MSAM.

References

[1] W. J. de Bruyn, Jeffrey A. Shorter, P. Davidovits, D. R. Worsnop, M. S. Zahniser, and C. E. Kolb. Uptake of gas phase sulfur species methanesulfonic acid, dimethylsulfoxide, and dimethyl sulfone by aqueous surfaces. *Journal of Geophysical Research: Atmospheres*, 99(D8):16927–16932, 1994.

[2] Lidia de Luca and Giampaolo Giacomelli. An easy microwave-assisted synthesis of sulfonamides directly from sulfonic acids. *The Journal of organic chemistry*, 73(10):3967–3969, 2008.

[3] B. B. Hicks and P. S. Liss. Transfer of so2 and other reactive gases across the air—sea interface. *Tellus*, 28(4):348–354, 1976.

[4] A. Lana, T. G. Bell, R. Simó, S. M. Vallina, J. Ballabrera-Poy, A. J. Kettle, J. Dachs, L. Bopp, E. S. Saltzman, J. Stefels, J. E. Johnson, and P. S. Liss. An updated climatology of surface dimethlysulfide concentrations and emission fluxes in the global ocean. *Global Biogeochemical Cycles*, 25(1):n/a–n/a, 2011.

[5] P. S. Liss and P. G. Slater. Flux of gases across the air-sea interface. *Nature*, 247(5438):181–184, 1974.

[6] Xiaoxi Liu, Benjamin Deming, Demetrios Pagonis, Douglas A. Day, Brett B. Palm, Ranajit Talukdar, James M. Roberts, Patrick R. Veres, Jordan E. Krechmer, Joel A. Thornton, Joost A. de Gouw, Paul J. Ziemann, and Jose L. Jimenez. Effects of gas–wall interactions on measurements of semivolatile compounds and small polar molecules. *Atmospheric Measurement Techniques*, 12(6):3137–3149, 2019.

[7] Demetrios Pagonis, Jordan E. Krechmer, Joost de Gouw, Jose L. Jimenez, and Paul J. Ziemann. Effects of gas–wall partitioning in teflon tubing and instrumentation on time-resolved measurements of gas-phase organic compounds. *Atmospheric measurement techniques*, 10(12):4687–4696, 2017.

[8] Cathleen Schlundt, Susann Tegtmeier, Sinikka T. Lennartz, Astrid Bracher, Wee Cheah, Kirstin Krüger, Birgit Quack, and Christa A. Marandino. Oxygenated volatile organic carbon in the western pacific convective center: ocean cycling, air–sea gas exchange and atmospheric transport. *Atmospheric Chemistry and Physics*, 17(17):10837–10854, 2017.

[9] S. E. Schwartz. Factors governing dry deposition of gases to surface-water. In S. E. Schwartz and W. G.N. SLINN, editors, *PRECIPITATION SCAVENGING AND ATMOSPHERE-SURFACE EXCHANGE, VOLS 1-3*, pages 789–801, NEW YORK, 1992. HEMISPHERE PUBL CORP.

[10] M. Yang, R. Beale, P. Liss, M. Johnson, B. Blomquist, and P. Nightingale. Air–sea fluxes of oxygenated volatile organic compounds across the atlantic ocean. *Atmospheric Chemistry and Physics*, 14(14):7499–7517, 2014.